Eindhoven University of Technology
Department of Electrical Engineering
Signal Processing Systems

TU/e technische universiteit eindhoven

Performance Validation of an IEEE 802.11a Receiver

By Luc Tan

Master of Science thesis

Project period: 6/2004 – 4/2006
Report Number: 0406

Commissioned by:
Dr. R. Rietman
PH.D. H.B. Zhang

Supervisors:
Dr. Ir. F.M.J. Willems

Additional Commission members:
Prof. Dr. Ir. J.W.M. Bergmans

Abstract

Wireless Local Area Networks (WLANs) were developed as a replacement for wired networks. They found their application in large data driven (TCP/IP) environments such as airports, conference-centers, and offices.

By now wireless products are more and more used in an in-home environment, e.g. for streaming-audio and video applications. However the WLAN standard was never intended for in-home operation and often these systems suffer from a lack robustness. To improve this robustness and to enhance the quality of service (QOS), diversity techniques are being developed.

The most commonly used diversity method is selection diversity. The receiver (and/or transmitter) here selects from a set of antennas the one that results in the best performance. Delay diversity is a second method. It can also be used by either the transmitter or the receiver or both. Delay diversity in principle creates frequency-selectivity in the transmission band and this improves the robustness (diversity) of a system.

Recently a real-time concept validator (RT-CV) for delay-diversity for IEEE 802.11a was developed and tested at Philips Research Laboratories. This RT-CV did not show any diversity gain however. The objective of this master's thesis project was to find out why the delay-diversity concept did not perform as well as was to be expected.

In the first part of this thesis-project we focussed on the expected performance of an IEEE 802.11a system under different transmission scenarios. This performance was obtained from Monte-Carlo simulation with a floating-point model of the system.

All functional blocks of the transmitter were already validated earlier and we therefore could assume throughout our investigations that the transmitter did not suffer from unacceptable performance degradation.

The next step was to validate the receiver. The first hardware block in the receiver that was tested was the analog digital (AD)-converter. From the measurements we could conclude that the converter suffered from severe performance degradation. Therefore the rest of the receiver-validation was done using an external AD-converter. Problems with this external AD-converter related to IQ-imbalance were solved using a delay element in one of the demodulator branches.

Finally the performance of the entire receiver-chain was measured. This resulted in the hypothesis that the receiver equalizer causes a significant performance degradation. This hypothesis was verified by simulations, by which we compare the implemented equalizer to two newly proposed implementations. We also suggest a modification of the de-mapper. As a result we could conclude that the performance degradation of the proposed implementations were acceptable for all the measurement scenarios, including delay diversity.

Table of contents

Chapter 1

Introduction

Current (wireless local area network (WLAN)) products are increasing in popularity. These systems were originally designed as a replacement of wired networks. As a result the WLAN standards do not comply very well with new applications. These new applications are e.g. the use of WLAN systems in mobile devices and in an in-home environment. To achieve better quality of service quality of service (QOS) several diversity methods were added to the system.

1.1 Background

The current IEEE 802.11a/g WLAN standard is developed for wireless data transfer, in large environments i.e. offices, airports, and conference centers. These WLAN systems are now more and more used in a home environment. There are several products available, which aim at improving the reliability of a WLAN connection in a home environment. An example of this is the Netgear Rangemax technology, which uses 7 antennas to achieve better performance (see website [1]).

One of the Philips strategies is the "Connected Planet" strategy, which foresees that the standard wireless technology is also used for distributing real-time streaming multimedia data, within an in-home environment. A major discrepancy between the standard IEEE 802.11a system and the "Connected Planet" strategy is that the IEEE 802.11a system was never developed for these applications. One of the problems of this standard is the bad QOS.

The requirements for this sort of applications are much more stringent than the requirements for TCP/IP-based data. The allowed outage or packet-error-rate packet error rate (PER) for audio video (AV) data is order of magnitudes lower than for data-transfer. No retransmissions are possible if we want to achieve a large enough throughput for these applications. In this project we will focus on the performance improvement, with respect to robustness of the physical layer of a IEEE 802.11a system, for use in a home environment.

A method to increase robustness is the use of multiple antennas at transmitter and receiver side. The experimental deliverable is an approved real-time concept validator (RT-CV) that performs different diversity techniques. This project will be based on an IEEE 802.11a system, but the results can also be used as input for the new high data rate standard IEEE 802.11n.

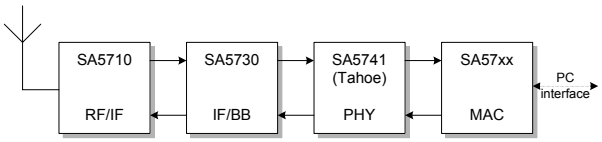

Figure 1.1: The first Philips IEEE 802.11a system.

1.2 History of the Project

In 1998 the System Laboratory Eindhoven (SLE) of Philips Semiconductors started with the development of WLAN products. The main goal was to create a total system solution for a wireless IEEE 1394 link. This project is called "Wireless IEEE 1394". The first demonstration of such a wireless IEEE 1394 link was presented at the IFA 1999 in Berlin (see announcement [33]).

One of the WLAN projects within the SLE was the development of an IEEE 802.11a and HIPERLAN/2 compliant base-band processor. This project was called the TAHOE project and it resulted in a test chip: the SA5741. Figure 1.1 shows a system overview of the whole IEEE 802.11a system, which was scheduled within Philips Semiconductors.

This IEEE 802.11a system was never developed. The SA5710 is the RF/IF chip, this chip modulates and demodulates the signals from 5.xGHz to an IF. This chip was not developed within Philips Semiconductors and the supplier (Lucent/Agere) did not deliver these chips. The SA5730 is the IF/Baseband chip; it was developed for Lucent/Agere. The SA5730 had a few tape-outs but did not meet the specification. The development of the medium access control (MAC) SA57xx chip was never started.

In 2002 the Tahoe project survived because of the need of an IEEE 802.11g OFDM physical layer. Together with the then developed IEEE 802.11b system, within Semiconductors, a pre IEEE 802.11g could be delivered. This system was never finished on time and was cancelled finally. As a result of these projects only one batch of SA5741 (or Tahoe chips) was produced. In this thesis this chip will be called Tahoe.

In the Tahoe project I participated in the developments of the synchronization algorithms and the top-level simulation model. In 2003 SLE closed and I became an employee of Philips Research. I participated in a new project in which a demonstrator for Ir. Wim van Houtum had to be developed. The demonstrator was based on the Tahoe chips and it had to show the performance gain of several diversity methods in real-time. This project was not meant to get exact performance numbers, but it had to show the gain in quality.

One of the main targets of the RT-CV was to demonstrate several diversity techniques on the corporate research exhibition (CRE) 2004. We managed to get the demonstrator working, but it did not show any performance advantage of these diversity techniques over conventional systems. We decided not to show this demo on the CRE. This was the starting point of my master's thesis project. The main objective of my thesis was to figure out why these methods did not give performance gain in the RT-CV.

1.3 Project Objective

The hardware did not produce the expected performance for delay-diversity. The project goal is to find out, why the RT-CV is not showing any performance gain. This is done based by performing measurements, simulations, and doing analysis. If necessary modifications of the current implementation have to be proposed and evaluated.

1.4 Outline

This document consists of a total of six chapters. This introduction is followed by Chapter 2, which provides the necessary background information on the IEEE 802.11 WLAN standard. In Chapter 3 the expected performance of the IEEE 802.11a physical layer is discussed. The measurement techniques and results are discussed in Chapter 4. This Chapter deals mainly with analog digital (AD)-conversion and IQ-imbalance. As results from these measurements a new equalizer was proposed. Chapter 5 discusses the currently implemented equalizer and proposes a new equalizer. Chapter 6 will draw conclusions and give recommendations for future work.

Chapter 2

IEEE 802.11 Standard

This chapter summarizes the background information on the IEEE 802.11 standard and the relation between the different layers of transmission. The last section of this chapter will focus on the IEEE 802.11a physical layer. This physical layer is also used in the IEEE 802.11g standard.

2.1 Standard Overview

One of the first standards for wireless local area network (WLAN) was the IEEE 802.11 standard. This standard is an extension of the wired-network standards. All IEEE 802 standards share their logical link control protocol, but they have a different medium access control (MAC) layer, each specialized to a specific physical layer and transmission medium. For more details see Figure 2.1, were on the left side we can see the IEEE 802 references and on the right side the ISO references. (Tanenbaum [26, p. 292-302])

2.1.1 Medium access control

The initial IEEE 802.11 standard consists of two parts. The first part is the MAC and is part of the data link layer of the ISO reference model. The MAC provides services such as authentication, privacy, association, distribution, integration and medium access. The IEEE 802.11 MAC corresponds to two types of wireless communication configurations.

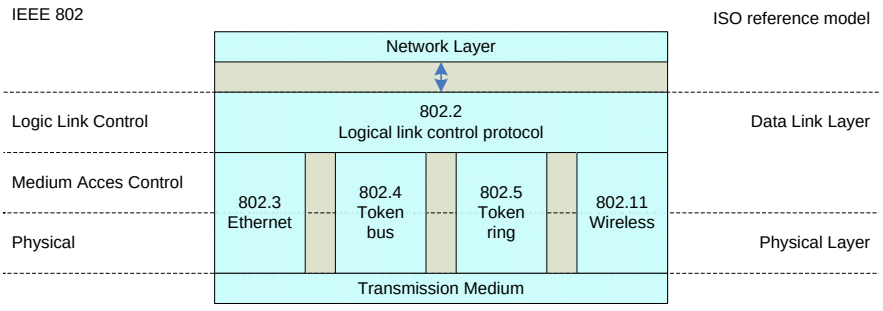

Figure 2.1: IEEE802-standard overview.

The first configuration is the independent communication case or the so-called ad-hoc network. The stations communicate with each other directly without any access-point. This configuration is very limited in size.

The other configuration is the infrastructure mode. In this mode there is an access-point that controls the communication. This access-point is connected to the wired network and will coordinate the wireless-network and give access from the wireless network to the wired network. In this mode the access point controls the channel. There are different MAC extensions for the IEEE 802.11 standard but that is out of the scope of this thesis.

2.1.2 Physical layer

Initially the IEEE 802.11 standard was defined for radio frequency (RF) based modulation and infra-red (IR) based modulation. Infrared communication is base-band oriented, while the RF modulation operates in the industrial scientific and medical (ISM) band of 2.4 GHz. For the RF layer, two modulation types were specified, frequency hopping spread spectrum (FHSS) and direct sequence spread spectrum (DSSS). In all three different physical layers a bit-rate of 1 and 2 Mbit/s is specified. Note that these Physical layer (PHY)s cannot communicate with each other.

FHSS is a well-known modulation method. This method is used in other standards such as Bluetooth. The data is modulated on a carrier and this carrier is hopping in the 2.4GHz ISM band. The 2.4GHz ISM band is split into 75 bands of 1MHz were the modulated carrier exists. The 802.11 standard provides a minimum hopping speed of 2.5 hops/s. The sender and receiver will have the same hopping scheme. The standard provides 22 hop patterns.

DSSS is developed in the army, for secure communication. The information is spread over a wide band and can be regarded as noise for the other receivers. In this standard a length 11 Barker code is used as spreading code. The crucial property of this code is, that it has good correlation performance. The spreading with a factor 11 gives the system robustness against narrow band interferers and short delay spreads. The 2.4GHz ISM band is split into fourteen 22MHz bands, some of these bands are overlapping each other. The data in the 1Mbit/s mode is modulated on the Barker sequence, with differential binary phase shift keying (DBPSK), were 2Mbit/s mode uses differential quadrature shift keying (DQPSK).

Higher bit-rates were needed for the WLAN standard, to meet the same capabilities as standard wired network. Therefore the standard IEEE 802.11 was extended with several higher data-rate modes. The first important extension was IEEE 802.11b.

The IEEE 802.11b extension of the standard was based on the DSSS physical layer of IEEE 802.11 standard and was backwards compatible with that standard. This extension adds two extra bit-rates to the standard bit-rates. These are 5.5MBit/s and 11MBit/s bit-rates. These modes do not use the Barker sequence as spreading code, but use complementary code keying (CCK) (see O'Hara [17, p. 148]).

Parallel to the development of the IEEE 802.11b systems, the development of the IEEE 802.11a standard started. This standard was not intended to be backwards-compatible with any other IEEE 802.11 physical layers. The idea was to make a physical layer, with a high bit-rate and special for the 5.xGHz band. Initially, this standard was not very popular due to the high cost of 5.xGHz components and lack of backwards-compatibility. In this project an IEEE 802.11a compliant system is used as basis vehicle for doing tests, with different diversity schemes. The new IEEE 802.11n standard would preferably use the 5.xGHz band.

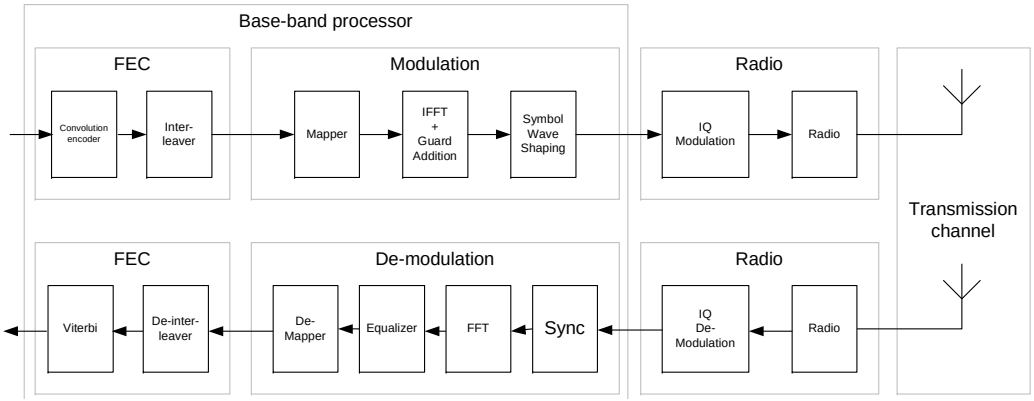

Figure 2.2: Concept block diagram of an IEEE 802.11a System.

The IEEE 802.11b products became very popular, because cheap 2.4GHz components were already available. There was also the need for higher data-rate products. The IEEE 802.11a base-band is used to get higher data-rates in the 2.4GHz ISM band. This standard results in the IEEE 802.11g standard, which is backwards compatible with IEEE 802.11b standard and uses the same modulation as the IEEE 802.11a standard.

A new standard will be IEEE 802.11n. This standard will be used in 5.xGHz band and also in the 2.4GHz ISM band. The major improvement of this standard is not only the higher channel bandwidth, or higher order modulation method, but the introduction of multiple-antenna systems. IEEE 802.11n provides higher bit-rates and/or more robustness using the concept of multiple input multiple output (MIMO).

2.2 Details IEEE 802.11a Physical Layer

The IEEE 802.11a standard is a WLAN standard for the 5.xGHz band. The IEEE 802.11g standard is a comparable standard for the 2.4GHz ISM band; it is a high-speed extension, which provides backwards compatibility with IEEE 802.11b standard. In this section we will present specific details about the IEEE 802.11a standard. Only the subjects that are relevant for this thesis will be discussed obviously.

Figure 2.2 shows the concept block diagram of an IEEE 802.11a system. In this section we will give a detailed description of the base-band processing operations. The radio and transmission channel will be discussed in 3.1 on page 20. The applied receiver algorithms will be discussed in Chapter 4 on page 35.

2.2.1 Forward error correction

The data-bits, which will be encoded in the forward error correction (FEC), are scrambled. This means that the data bits are randomized by adding a pseudo random bit sequence (PRBS) to them. The probability that a bit will be logical zero or logical one is equal. This scrambling algorithm avoids long sequences of logical zeros or ones.

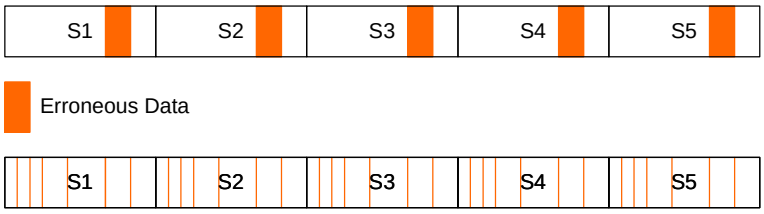

Figure 2.3: Interleaver.

The data bits are spread over different sub-carriers, this gives frequency diversity. If we want to have a robust transmission, there must be redundancy in the signal. The redundancy is added to the signal with convolutional code. The possible code rates in an IEEE 802.11a system are 1/2, 2/3 and 3/4. This means e.g. for code-rate 1/2 that the number of coded bits is 2 times the number of data (information) bits.

A Viterbi decoder performs the decoding operations. This decoder will try to recover the transmitted data bits using the redundancy among the code bits and the channel information. More information about Viterbi decoding can be found in Proakis [21, p. 471] and Haykin [13, p. 195].

We speak about a fade when a group of subsequent sub-carriers has a small signal to noise ratio. This means that a block of received data within an OFDM symbol will be unreliable. The Viterbi decoder cannot handle such a burst-errors very well; therefore the data is pseudo-randomly distributed over the sub-carriers. This process is called interleaving (see Figure 2.3).

2.2.2 Modulation

The data (bits) are modulated with the following modulation schemes: BPSK (1-bit per symbol), QPSK (2-bits per symbol), 16-QAM(4-bits per symbol) and 64-QAM (6-bits per symbol). This means that the number of bits per sub-carrier can vary form 1 up-to 6 bits.

After the mapping there will be an orthogonal frequency division multiplexing (OFDM) modulator, which is an inverse discrete Fourier transform (IDFT) operation. In the IEEE 802.11a standard the number of sub-carriers is 64. An OFDM symbol is calculated with a 64-points inverse fast Fourier transform (IFFT). The sample frequency is 20MHz, this means that the frequency spacing of each sub-carrier is $20MHz/64 = 312.5KHz$.

An OFDM symbol consists of 64 sub-carriers and also 64 time-domain samples of 20MHz. Therefore the OFDM symbol duration is $3.2\mu s$. In IEEE 802.11a the cyclic prefix (or guard interval) occupies one fourth of the OFDM symbol duration, hence it is $0.8\mu s$ long. The total OFDM symbol duration of an IEEE 802.11a OFDM symbol will consequently be $4\mu s$.

Not all the sub-carriers are used for data transmission. Figure 2.4 shows the spectrum of an OFDM symbol of an IEEE 802.11a system. The left- and rightmost carriers of the symbol are not used for transmission. This is done to make filtering more easy. There are four pilot carriers which can be used for common phase error (CPE) correction. The pilot carriers are modulated with known sequences of data. The remaining 48 sub-carriers are used for actual data transmission.

The last part of the base-band processor transmitter is devoted to symbol-wave shaping. In the standard [25, p. 29] a spectral mask is defined. If the output of the IDFT is not shaped, then

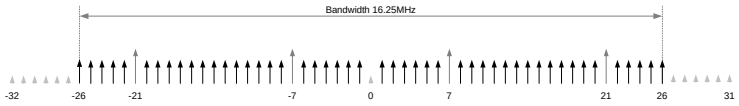

Figure 2.4: IEEE 802.11a used spectrum.

filtering the signal is necessary to meet this requirement. To reduce the complexity, instead of an analog filter, symbol-wave shaping is applied in the digital domain. In the Tahoe chip we find a sample-rate converter, which over-samples the signal by a factor of two. Filtering this over-sampled signal is relatively simple.

2.2.3 Preamble and signal field

Unlike DVB-T and DAB, an IEEE 802.11a system transmits in bursts. The receivers in the WLAN network have to synchronize to these bursts and decode them correctly.

In streaming applications the receiver could take a number of OFDM symbols and do the synchronization algorithms on these symbols. Algorithms such as automatic gain control (AGC), time and frequency recovery are done based on these symbols. These algorithms are based on the fact that the cyclic prefix is a copy of a part of the OFDM symbol and the correlation between these parts can be used to synchronize.

In burst transmission systems, the receiver does not synchronize on a number of OFDM symbols. Instead, it synchronizes on a so-called preamble. The preamble is a training sequence, which is known at the receiver. There is no data embedded in this preamble. The preamble consists of two parts. The first part is called the short training sequence. This short training sequence (of $8\mu s$) is used for AGC and coarse time and frequency recovery. The second part is called the long training sequence. This portion is used for channel estimation and fine time and frequency recovery. The long training sequence contains two OFDM symbols and a cyclic prefix. In the standard [25, p. 12 f. 110] it is proposed, how to use the preamble for synchronization. In the Tahoe a method different from the proposed one is used.

The received signal $r(t)$ can be calculated like Equation 2.1. This received signal contains the transmitted signal $s(t)$, which is convolved with the channel response $h(t)$. The receiver knows the transmitted sequence $s(t)$. It does not know the channel response $h(t)$ and the noise $n(t)$. The receiver now has to estimate the channel response and the noise power ($E(NN^*)$). This can be obtained from the long training sequence. For estimation of the noise power see Subsection 5.2.3 on page 52.

$$r(t) = (h * s)(t) + n(t), \tag{2.1}$$

$$(h * s)(t) = \int h(\tau)s(t-\tau)d\tau, \tag{2.2}$$

$$R(\omega) = H(\omega)S(\omega) + N(\omega). \tag{2.3}$$

The channel response is estimated in the frequency domain. Equation 2.3 shows the Fourier transform of the received signal. If $S(\omega)$ is known, then the channel response can be estimated from the received signal $R(\omega)$.

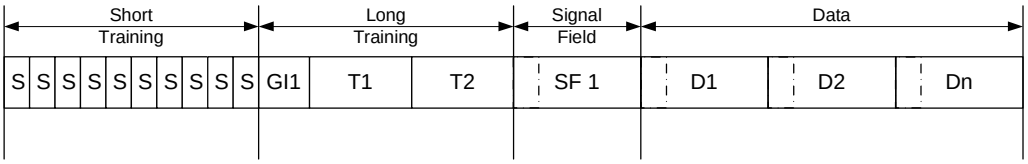

Figure 2.5: IEEE 802.11a framing structure.

Data rate (Mbits/s)	**Modulation**	**Coding rate (R)**	**Coded bits per subcarrier (N_{BPSC})**	**Coded bits per OFDM symbol (N_{DBPS})**	**Data bits per OFDM symbol (N_{DBPS})**
6	BPSK	1/2	1	48	24
9	BPSK	3/4	1	48	36
12	QPSK	1/2	2	96	48
18	QPSK	3/4	2	96	72
24	16-QAM	1/2	4	192	96
36	16-QAM	3/4	4	192	144
48	64-QAM	2/3	6	288	192
54	64-QAM	3/4	6	288	216

Table 2.1: Data rates from the IEEE 802.11a standard.

$$\hat{H}(\omega) = \frac{R(\omega)}{S(\omega)} = \frac{H(\omega)S(\omega) + N(\omega)}{S(\omega)} = H(\omega) + \frac{N(\omega)}{S(\omega)}. \tag{2.4}$$

Note that the estimated $\hat{H}(\omega)$ contains noise. The long-training sequence contains two training OFDM-symbols. If we use both of these training symbols the quality of the estimated channel response is improved.

2.2.4 Overview

After the preamble a signal field is transmitted. This field contains the number of bytes and the data rate used in the following transmissions. It is modulated with BPSK, code-rate 1/2. The whole frame structure is depicted in Figure 2.5

Table 2.1 summarizes all the data-rates, which are defined in the standard. For each data-rate, modulation and coding parameters are specified.

Chapter 3

Expected Performance of the Receiver

The Physical layer (PHY) is used as transport of bytes from point to point. The PHY has no knowledge of any network or protocol. The medium access control (MAC) provides the PHY not only with the transmitted data, but it will also give information about bit-rate and some other additional information (for more information see Tanenbaum [26, Sec. 4.4.3]). Figure 3.1 shows the block diagram of a PHY. The first is the forward error correction (FEC) the second is the modulation; the last is the radio and transmission channel. The transmission channel is the only part that the system cannot control; all the other parts are designed to get bit-error free transmission. In this thesis we use an equivalent complex base-band channel model for the radio and transmission channel.

This chapter consists of four sections. The first section will give a brief introduction into channel characteristics. The channel is unknown but measurements are done to statistically characterize this channel. The second and third section contains a description of the performance of the PHY in combination with an additive white Gaussian noise (AWGN) channel and in a flat-fading channel situation. In the last section we will introduce several diversity methods and in this section we will give performance results for several diversity methods. The results that are obtained from this chapter will be used as reference for the next two chapters.

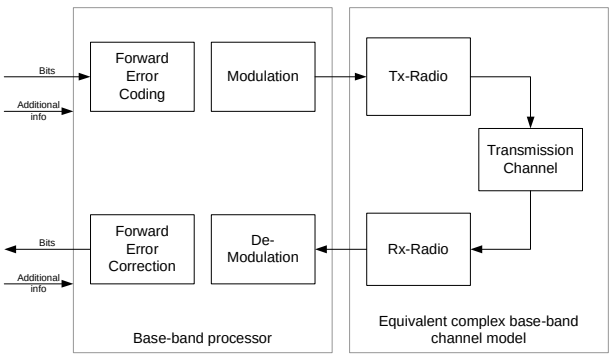

Figure 3.1: Physical layer overview.

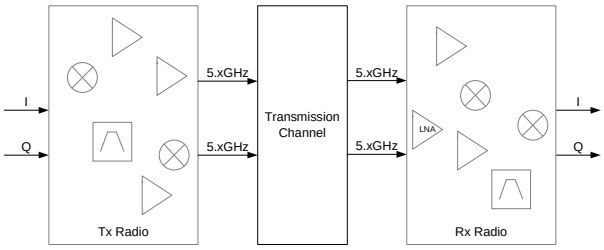

Figure 3.2: Block diagram of transmission channel.

3.1 Channel Characteristics

A transmission channel can be statistically characterized. This section deals with the analog radio that modulates, filters and amplifies the signal. If we talk about the transmission channel, it includes the radio. Therefore we will use in our discussions a complex equivalent base-band channel model. Figure 3.2 depicts a block diagram of this transmission channel. In this model there are two transmitting antennas and two receiver antennas. The transmission channel can be seen as a MIMO channel. The real-time concept validator (RT-CV) is a 2x2 multiple input multiple output (MIMO) system. In this thesis (see Subsection 3.1.3 on page 25) only SISO and SIMO scenarios are defined.

In this thesis we have a single base-band signal and multiple antennas. In the analog domain these multiple antenna signals are created in the transmitter. In the receiver these multiple antenna signals are combined at IF such that they result in a single base-band signal. This means that this system does not need multiple analog digital (AD) and digital analog (DA) converters unlike other MIMO system, such as Institute of Electrical and Electronics Engineers (IEEE) 802.11n. Therefore this system is sometimes called "poor-man's MIMO".

There are two channel effects in this system; the first effect is noise that is added to the signal. This noise is mainly due to the analog radio components. The second effect is multi-path fading; this comes from the transmission channel. These two effects will be discussed in the following two subsections.

3.1.1 Noise

In this subsection we will take as example an AWGN channel. The aim of this part is to find out, which parts contribute to the total noise that can be observed at the input of the base-band processor.

The AWGN channel model is a simple channel model. This model is used for a first verification of the performance. Equation 3.1 contains the mathematical description, which is used in the equivalent complex base-band channel model. In this equation $r(k)$ is the complex received signal, $s(k)$ is the complex transmitted signal and $n(k)$ is complex white Gaussian noise. Variable k is the sample index and K is the number of samples of a IEEE 802.11a frame.

$$r(k) \quad = \quad s(k) + n(k), \qquad k = 0..K-1 \tag{3.1}$$

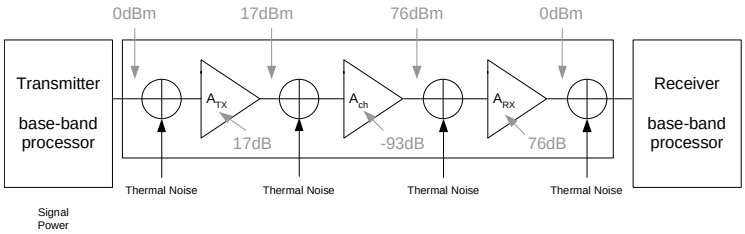

Figure 3.3: Thermal Noise.

$$SNR = \frac{P_s}{P_n} = \frac{1/K \sum_{k=0}^{K-1} s(k)s^*(k)}{\frac{52}{64} 1/K \sum_{k=0}^{K-1} n(k)n^*(k)}. \tag{3.2}$$

The signal to noise ratio (SNR) can be calculated by dividing the power of the transmitted signal by the noise power. It is clear form the spectrum of IEEE 802.11a orthogonal frequency division multiplexing (OFDM) symbol (see Figure 2.4) that not all the sub-carriers are used. The used data carriers and pilots only contribute to the power of the signal. This means that the bandwidth of the signal is smaller than the bandwidth of the noise. To correct this the noise is scaled with a factor of $\frac{52}{64}$.

If we decompose the radio and channel into gain blocks, then the system looks like Figure 3.3. With the Friis transmission equation the gain distribution can be calculated (see Haykin [13, p. 18-19]). Figure 3.3 shows a realistic example of the gain distribution. In this example there is a path loss of $-93dB$.

The FCC regulations require that the maximum transmitted power in the lower band of the 5.xGHz band is $17dBm = 50mW$, this is also a practical value for the average transmitted power. In the receiver there is automatic gain control (AGC), which will prevent the AD converter in the base-band processor from clipping. This means the gain of the receiver is variable depending on the received signal strength.

All parts in the channel suffer from thermal noise. This thermal noise power can be calculated with the formula of $K \cdot T \cdot B$, were K is the Boltzman constant, T the temperature ($290^\circ K$) and B the noise-bandwidth ($18MHz$ see the standard [25, p. 29]) of the signal. In this case the power of the thermal noise is $-101dBm$. If we use the model in Figure 3.3, the SNR at the output of the channel can be calculated.

$$SNR_{rx} = \frac{A_{tx}A_{ch}A_{rx}P_{tx}}{(A_{tx}A_{ch}A_{rx} + A_{ch}A_{rx} + A_{rx} + 1)P_{Noise}}, \tag{3.3}$$

$$= (1 + \frac{1}{A_{tx}} + \frac{1}{A_{tx}A_{ch}} + \frac{1}{A_{tx}A_{ch}A_{rx}})^{-1} \frac{P_{tx}}{P_{Noise}}. \tag{3.4}$$

In this equation the term with the smallest argument, will have the largest contribution to the SNR. If we take the example from Figure 3.3, then the term $\frac{1}{A_{tx}A_{ch}}$ has the largest contribution to the SNR. This means that thermal noise source in front of the amplifier A_{rx} is dominant. It is clear that the wanted signal power is minimal at this point. If we neglect all the other thermal noise sources the SNR can be approximated as follows:

$$SNR_{rx} \approx \frac{P_{tx}}{P_{Noise}(\frac{1}{A_{tx}A_{ch}})}, \tag{3.5}$$

$$SNR(dB)_{rx} \approx P(dBm)_{tx} - P(dBm)_{noise} + A(dB)_{tx} + A(dB)_{ch} = 25dB, \tag{3.6}$$

$$\approx 0dBm + 101dBm + 17dB - 93dB = 25dB. \tag{3.7}$$

The SNR is linear with the received input power, in case the signal at the input of the receiver is the minimal power in the transmission channel. The calculation includes only thermal noise. This thermal noise is generated by passive elements in the circuit. Amplifiers in the circuit also generate noise. The amount of noise that these amplifiers generate depends on the construction of the amplifier (see Haykin [13]). This effect is also called noise figure of an amplifier. In the standard [25, p. 31] a receiver noise figure of 10dB is mentioned. If we use this 10dB in this example then we obtain a SNR of 15dB (see equation 3.8). This is also called the Friis noise equation.

$$N(dBm)_{rx} = N(dBm)_{irx} + A(dB)_{rx} + Fdb \tag{3.8}$$

$$= -101dBm + 76dB + 10dB = -15dBm, \tag{3.9}$$

$$SNR(dB)_{rx} = P(dBm)_{tx} + A(dB)_{tx} + A(dB)_{ch} + A(dB)_{rx} - N(dBm)_{out} \tag{3.10}$$

$$= 0dBm + 17dB - 93dB + 76dB + 15dBm = 15dB. \tag{3.11}$$

With these formulas we can calculate the resulting SNR at the input of the base-band processor including an AGC loop. Figure 3.4 shows the gain distribution of the system for different receiver input power levels ($P_{irx} = P_{tx}A_{tx}A_{ch}$). In this system transmitted power P_{tx} and transmitter gain A_{tx} are constant. The first curve is the resulting SNR at the base-band processor. The second curve is the gain of the receiver A_rx for different input powers P_{irx}. The third curve is the input power of the receiver base-band processor ($P_{rx} = P_{tx}A_{tx}A_{ch}$). This power must not exceed the $0dBm$. If this value exceeds the $0dBm$ the AD could clip. The AGC will adjust the receiver gain (A_{rx}) in such a way that this would not occurs. The noise power at the input of the receiver base-band processor will be ($N_{rx} = N_{irx}A_{rx}F$). The F is the noise figure of the receive amplifier (10dB).

The transmitted signals are not perfect. The major problem here is not noise, but the harmonic distortion. In practice we may assume that the quality of the transmitted signal is much better than the noise in the receiver. Therefore we assume in this thesis that the transmitter is perfect.

As conclusion the noise from the AWGN channel has got a direct relation with the received signal strength. The noise in the radio chain depends on thermal noise and the quality of the amplifiers in the chain, in terms of noise figure.

3.1.2 Multi-path fading

"Multi-path fading" is bipartite, multi-path and fading. Multi-path means that the receiver receives multiple transmitted signals, via different transmission paths. Multi-path gives frequency selectivity in the received signal. The fading means that the channel is varying in time, although this is not so relevant for transmission of a single packet.

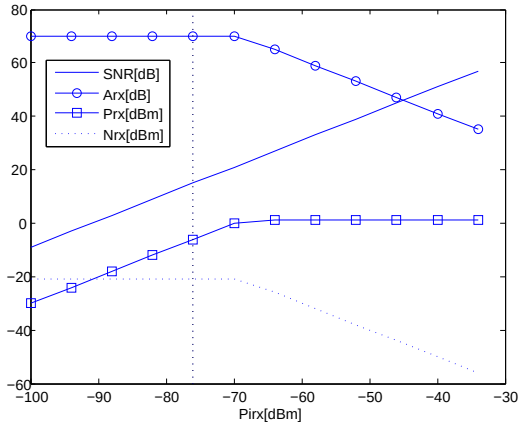

Figure 3.4: Effect of input power vs SNR after AD conversion.

One of the strengths of OFDM is, that it is robust against multi-path fading. Every transmission path has a specific path loss and delay. Equation 3.12 is an example of a multi-path effect consisting of N transmission paths. The path-loss is represented by complex number h_n and the delay by τ_n. This equation contains the received signal $r(t)$ without noise.

$$r(t) = \sum_{n=0}^{N-1} h_n s(t + \tau_n). \tag{3.12}$$

The Fourier transform of this received signal is given by:

$$R(\omega) = S(\omega) \sum_{n=0}^{N-1} h_n e^{(\jmath\omega\tau_n)}. \tag{3.13}$$

From this equation the channel frequency response can be calculated:

$$H(\omega) = \frac{R(\omega)}{S(\omega)} = \sum_{n=0}^{N-1} h_n e^{(\jmath\omega\tau_n)}. \tag{3.14}$$

An example of a multi-path channel response is:
$\tau_0 = 0$, $h_0 = 1$ and $\tau_1 = 100ns$, $h_1 = 1$. Figure 3.5 contains the power frequency channel response of this example. One property of this example is that the fades are 10MHz spaced from each other $(1/(\tau_0 - \tau_1))$.

Fundamental work on modelling indoor channels is published in Hashemi [11], Saleh [23]. In publication Chayat [5], these channel models are simplified in a fixed number of channel coefficients with equidistant delays. The different transmission paths resolve in these channel coefficients. The amplitudes of the channel coefficients are independent distributed Rayleigh variables and the phases are uniformly distributed. This leads to a channel model that contains a number of channel coefficients h_n (see equation 3.16). This channel model is a Rayleigh fading channel

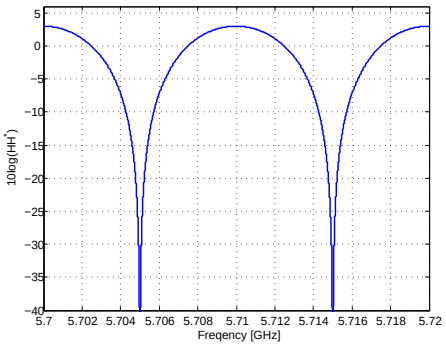

Figure 3.5: Example channel realization in frequency domain.

model, without a line-of-sight component. This is a worst-case scenario for an in-door wireless communication system.

$$r(k) = \sum_{n=0}^{N-1} h(n)s(k-n), \qquad k = 0..K-1, \tag{3.15}$$

$$h(n) = N(0, \sigma_n^2/2) + \jmath N(0, \sigma_n^2/2), \tag{3.16}$$

$$|h_n| = R(\sigma_n^2), \tag{3.17}$$

$$\arg(h_n) = U(-\pi, \pi). \tag{3.18}$$

The received signal $r(k)$ is a time discrete signal, with k as sample index. In equation 3.16 $N(\mu, \sigma_k^2)$ is a Gaussian or normal distribution, with a mean of 0 and a variance of σ_n^2. $R(\sigma_n^2)$ is a Rayleigh distribution and $U(-\pi, \pi)$ refers to a uniform distribution.

For indoor channel an exponential power-delay profile is expected. This exponential channel model is used for simulations. This model assumes those transmission paths are weaker onavarage, when they have longer path-length. This is in general not always true, but for modelling a wireless indoor channel this is a commonly used model. This channel model is used in the standard see O'Hara [17, p. 164].

Equation 3.19 is a description of this IEEE 802.11a channel model. The power is exponentially decreasing with the terms $e^{-kT_s/2T_{rms}}$, were T_s is the sample period and T_{rms} is the RMS power delay spread of the channel. The term σ_0 is used for normalizing the power.

$$h_n = \sigma_0 e^{-nT_s/(2T_{rms})}(N(0,1) + \jmath N(0,1))\sqrt{1/2}, \tag{3.19}$$

$$\sigma_0 = 1 - e^{-T_s/T_{rms}}. \tag{3.20}$$

In this theoretical model the number of channel coefficients will be infinity long. In simulations the number of channel coefficients is limited. Only the channel coefficient, which have a contribution larger than $-40dB$ will be used ($\sigma_0 e^{-nT_s/2T_{rms}} > 10^{-40/20}$).

The coherence bandwidth of the channel can be calculated from the RMS delay spread of the channel (see Equation 3.21). The coherence bandwidth is the bandwidth were two frequencies of

T_{rms} **[ns]**	BW_{coh} **[MHz]**	**Reference**	**Remarks**
40	12.5	Devasirvatham [6]	Large building (e.g., Stock Exchange)
50	10	Hafezi [10]	Office building
35	14.3		Meeting room (5m x 5m) with metal walls
10	50		Single room with stone walls
40	12.5	Devasirvatham [7]	Office buiding
40	12.5	Hawbaker [12]	Indoorsports arena
65	7.7		Factory
25	20		Office buidling
20	25	Nobles [16]	Office building: single room only

Table 3.1: Measured delay spreads in frequency range of 4 to 6 GHz.

a signal are experiencing correlated fading. For more information about coherency bandwidth see Haykin [13, p. 60].

$$BW_{coh} \approx \frac{1}{2T_{rms}}. \tag{3.21}$$

Empirical measurements are done on these multi-path fading effects in the 5.xGHz band. These measurements result in a typical channel profile for a certain environment. The results of different measurements are in Table 3.1 (van Nee [32, p. 19])

From Table 3.1 it is clear that the RMS delay spread of In-Home environment is very low. This means that the coherence bandwidth is larger than the bandwidth of an IEEE 802.11a signal ($16MHz$). Therefore we will use in this thesis a flat-fading channel model, for all simulations and measurements.

The last part of this section is the fading aspect. Fading means that the channel varies during the time. In this thesis we will assume that channel is slowly fading. This means that fading remains essentially unchanged during a transmission of each IEEE 802.11a frame. So the coherence time of a channel is much smaller than the duration of a single IEEE 802.11a frame. In simulations and measurements every IEEE 802.11a frame has its own channel realization.

3.1.3 Measurement scenarios

In this subsection there will be a brief introduction in the performance measurement scenarios, which are used in this thesis. As we know from the tests with the RT-CV, that the performance of delay-diversity is worse than expected. These scenarios have to determine whether the RT-CV is causing the performance degradation that we observe in the delay-diversity case. Moreover we should find out which specifuc parts of the RT-CV could cause the performance degradation. These scenarios are not studied to find out what the benefits are of different diversity methods.

Table 3.2 contains all the scenarios. The first measurement scenario is a SISO AWGN channel scenario. This scenario is used in van Houtum [30]. This is a relatively simple scenario, were only white Gaussian noise is added to the signal. This scenario gives an impression of what the system performance is. The second scenario is SISO flat-fading scenario, were there is no diversity applied.

MODE	Num Tx ant	Channel	Num Rx ant	Diversity method
SISO	1	AWGN	1	NA
SISO	1	Flat-fading	1	NA
SIMO	1	Flat-fading	2	selection
SIMO	1	Flat-fading	2	delay (100ns)

Table 3.2: Measurement scenarios.

This scenario will give the performance in small environments, with small RMS delay-spread. The third scenario is SIMO channel, with multiple receive antenna, were the best receiver antenna is selected (see Subsection 3.4.2 on page 31). This method is commonly used in the current WLAN cards. The last scenario is the delay-diversity scenario (see Subsection 3.4.3 on page 31). A delay of 100ns is applied to one of the receiver branches.

In the following sections the expected performance of these scenarios will be discussed. These scenarios will also be discussed in the next two chapters.

3.2 Performance of an AWGN Channel

In this section the performance of an IEEE 802.11a system in an AWGN channel situation will be presented. The results of this section will be used for the performance analysis of the other scenarios. This analysis will also be used as reference for the performance of the Tahoe chip.

If we consider an AWGN channel, all the sub-carriers of the OFDM symbol get the same amount of noise. This means that we can compare our OFDM system with a single carrier system. In the standard [25, p. 31] the packet error rate (PER) is defined for a packet of 8000 bits (1000 bytes) and required to be not larger than 10%. A packet is called erroneous if one or more bits are erroneous.

$$P_{PER} = 1 - P_{correct}, \tag{3.22}$$
$$P_{PER} = 0.1 \leftrightarrow P_{correct} = 0.9. \tag{3.23}$$

If we assume that bit errors are independent, then:

$$P_{correct} = (1 - P_{ber})^{8000}, \tag{3.24}$$
$$P_{PER} = 1 - (1 - P_{ber})^{8000}, \tag{3.25}$$
$$(1 - P_{ber})^{8000} = 0.9, \tag{3.26}$$
$$P_{ber} = 1 - 0.9^{1/8000} = 1.317 \cdot 10^{-5}. \tag{3.27}$$

In Dilling [8, p. 11] there is a table, which lists the required SNR to get a PER performance of 10% for different various modulation methods. The SNR is defined as $SNR = \frac{E\{|s|^2\}}{N_0}$. For 54Mbit/s a SNR of 19 dB is required. This SNR is defined before the FEC. Van Houtum [30]

Data rate (Mbits/s)	Minimum Sensitivity [dBm] [25, p.31]	Noise level [dBm]	SNR at antenna [dB]	SNR before FEC [dB]	Receive input SNR from Dilling and van Houtum
6	-82	-101	19	4	2.8
9	-81	-101	20	5	5.4
12	-79	-101	22	7	5.8
18	-77	-101	24	9	8.4
24	-74	-101	27	12	12
36	-70	-101	31	16	14.9
48	-66	-101	35	20	19.6
54	-64	-101	37	22	20.7

Table 3.3: Minimum required SNR at the input of the receiver.

indicates that there is 1.7dB loss due to the channel estimation in the equalizer (See Appendix A on page 77).

Table 3.3 shows the results of all the SNR calculations. The last column contains the SNR from Dilling [8] to which we add with 1.7dB. If we compare this performance with van Houtum [30, Fig. 4] at BER of $1.317 \cdot 10^{-5}$, the same SNR (20.7dB) can be obtained.

A second calculation can be done based on numbers, which can be found in the standard [25]. In the standard [25, p. 31] a minimum sensitivity is defined; this can be found in the second column of the table. In the standard [25, p. 31] a noise figure of 10dB and implementation loss of 5dB is suggested. So the loss between the receive antenna and the input of the receiver is around the 15dB. With this information the required SNR can be obtained. The difference between both the numbers is around 1dB.

The last study is the performance, which is simulated with a floating-point model. Monte-Carlo simulations are performed to get the exact performance of this IEEE 802.11a system. These simulations are done with floating-point models. The results of the 54Mbit/s simulation are in Figure 3.6. If we compare these with simulation results of van Houtum [29], then the same SNR is obtained for a 10% PER.

The calculation from Dilling [8] assumed that the bit-errors are independent. The simulation shows that this assumption is not true.

$$PER(SNR) = 1 - \left(1 - Q\left(\alpha\sqrt{SNR}\right)\right)^{8000} \tag{3.28}$$

In Figure 3.6 the simulation results can be found. The second curve is approximation of this simulation results. This approximation is done with a Q-function (see Equation 3.28) and is used to obtain the performance in the following sections. The Q-function can be used to obtain the bit-error rate. Equation 3.25 is used to obtain the PER. Variable α is set in such a way that these curves match. The same value of this variable is used in all the calculations which are done in the next subsections.

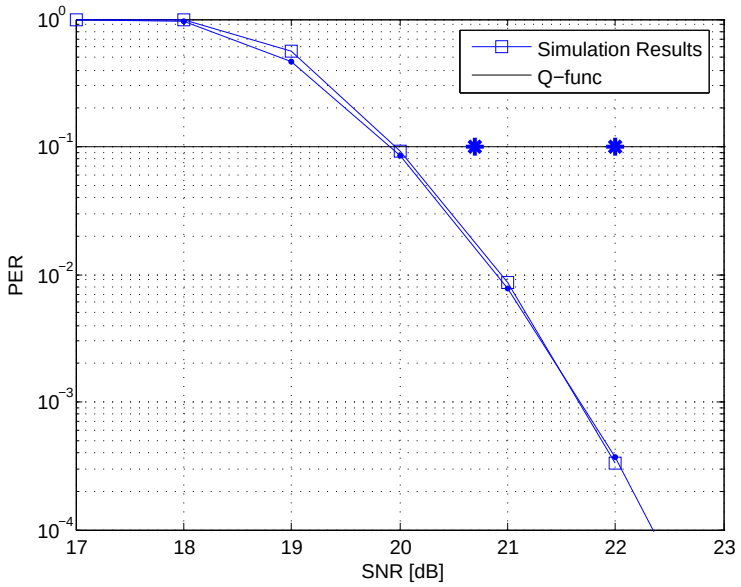

Figure 3.6: Performance of AWGN channel for 54Mbit/s.

3.3 Performance Flat-fading Channel

A flat-fading channel is a simple channel, with a single channel-coefficient. This coefficient is a complex coefficient whose magnitude has a Rayleigh distribution. It will be assumed, that it is constant through anIEEE 802.11a frame. Equation 3.29 shows this channel model.

$$r(k) \quad = \quad h_n s(k) + n(k) \qquad k = 1..K-1. \tag{3.29}$$

The performance of flat-fading channel could be obtained with different methods. In this thesis only Monte-Carlo simulations are done to obtain the performance of this system under flat fading. An other method (analytical calculation) can be found in e.g. Tse and Viswanath [27, p. 62/Eq. 3.37].

The first method is to take a sufficient number of channel realizations. Calculate for each channel realization the SNR_n. We assume that the variance of the channel coefficient is one ($E(hh^*) = 1$) and the variance of the noise will be increased depending on the wanted SNR ($SNR = E(SNR_n)$). The PER of each instant channel realization can approximated with a Q-function (see equation 3.28). The performance in terms of PER can now be calculated with equation 3.30.

$$PER(SNR) \quad = \quad \frac{1}{N} \sum_{n=0}^{N-1} (PER(SNR_n)). \tag{3.30}$$

The first curve in Figure 3.7 contains the results of the performance calculation, which is done with the Q-function. This is the performance, which is expected in an in-home environment, if

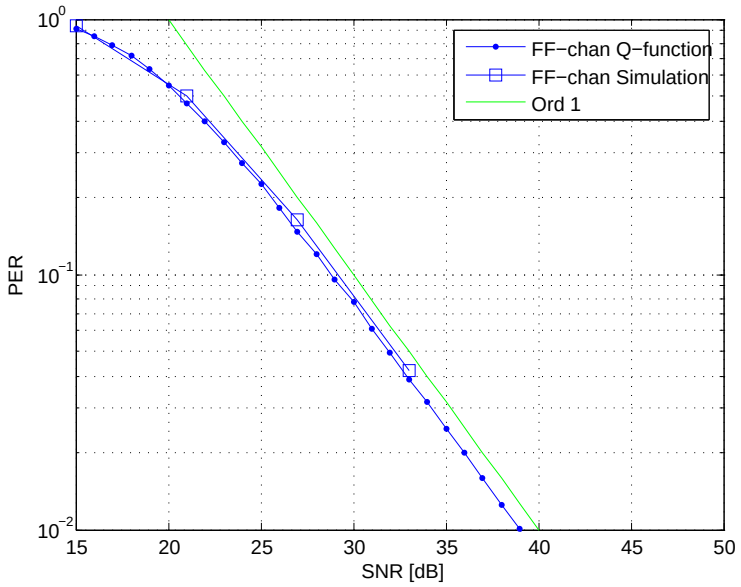

Figure 3.7: Performance of SISO flat-fading channel for 54Mbit/s.

there is no diversity applied to the system. The second curve in the figure contains the simulation results with floating-point model of this channel. It is clear that for high SNR this curve has a diversity order of one. Equation 3.31 shows the calculation of this curve, were L is the diversity order. This was expected from the analysis of Tse and Viswanath [27, p. 62/Eq. 3.37]. This curve is also plotted in the figure.

$$ORD_L(SNR) = \frac{1}{(\beta \cdot SNR)^L}. \tag{3.31}$$

3.4 Diversity Methods

As described in the previous section, the performance of an IEEE 802.11a system degrades very significantly in a flat-fading environment. From the statistical properties of the channel, as explained in Section 3.1 on page 20, it is clear that in some cases it is impossible to transmit data over a certain realized channel. Diversity methods may be used to get a better performance. This means that the receiver gets more information. There are several methods to create diversity. In this thesis three of these methods are described: time diversity, frequency diversity and space diversity.

In this section we will give an introduction of several diversity methods. The second subsection will discuss details about selection diversity. This method combines multiple receive antennas to a single base-band signal and is commonly used in IEEE 802.11a system. Monte-Carlo simulations are done to determine the performance of these diversity methods. In the last subsection of this section there will be an introduction into delay diversity methods. These method are simulated in

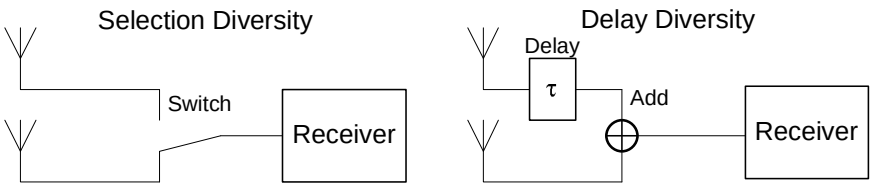

Figure 3.8: Block-diagrams of two diversity methods.

Matlab. Delay diversity is a combination of frequency diversity (creating frequency selectivity in a flat-fading channel) and space diversity (multiple antennas).

3.4.1 Some diversity methods

The first diversity method is time diversity. Time diversity means that certain data are repeated in different time slots. This gives the receiver the opportunity to receive the same information multiple times. In a well-designed system there will be at least one packet successfully received. This method of diversity will decrease the throughput, but it enhances the robustness and it does not need any additional hardware.

The second method is frequency diversity, which means that the same data is transmitted at the same time but on different frequencies. As a result, the bandwidth of the transmitted signal is larger than strictly needed for transmission. The throughput of the data remains the same, but the bandwidth of the system will be higher. A method to create such diversity is coded orthogonal frequency division multiplexing (COFDM). The coded bits are spread over different sub-carriers of an OFDM symbol.

Frequency diversity will be beneficial if the coherence bandwidth is smaller then the total bandwidth of the signal. In case of in-home environment coherence bandwidth is typical larger than the bandwidth of an IEEE 802.11a system. The signal bandwidth of an IEEE 802.11a system is around 16.5MHz, if the zero sub-carriers of OFDM symbol are not taken in account. Table 3.1 shows that the coherence bandwidth of small environments is larger than the signal bandwidth of the IEEE 802.11a signal. COFDM modulation will therefore not give any frequency diversity gain in an in-home environment.

The last diversity method is space diversity. Just as frequency and time, space could also be used to get diversity. Such a system contains multiple transmit and receive antennas. If the transmission channels between the different antennas are assumed to be uncorrelated, then there will be a diversity gain. In this thesis we will always assume uncorrelated transmission channels. This diversity method is often referred to as a MIMO system. In most of the cases a MIMO systems contains multiple front-ends and AD and DA converters. A special case of such a MIMO system is a SIMO system, which uses single transmit antenna and multiple receive antennas. This system is used in the measurement scenarios. The other special case is a MISO system with multiple transmit antennas and single receive antenna. Alamouti [4] coding is a well-known method for transmission over such a system.

3.4.2 Selection diversity

In wireless local area network (WLAN) OFDM systems various diversity methods are possible. The most commonly used method is selection diversity. This diversity method is am implementation of spatial diversity. Figure 3.8 shows a block diagram of this diversity method. The receiver has to determine which receive antenna is the best and selects that antenna. One selection criterion could be based on the power of an antenna. This is implemented in the RT-CV. If the channel is a flat-fading channel, this selection criterion will give the optimum performance. Equation 3.33 is the mathematical description of selection diversity based on the power of the channel response of a flat-fading channel.

$$i = argmax(h_k h_k^*), \tag{3.32}$$

$$r_{sel}(t) = h_i s(t) + n_i(t). \tag{3.33}$$

There are practical issues related to the implementation of this method in a real system and also in the RT-CV. We mention here the timing-issue, i.e. to pick the time when to make a selection. If the system makes a selection while receiving an IEEE 802.11a frame, this will give frame errors. If a selection is made between the frames we do not get information about the channel parameter. The decision is therefore made in the short training sequence. The other practical issue of this method of creating diversity is how to find the best receive antenna. This is done in the RT-CV, with two power detectors, one on each antenna.

The PER curve of selection diversity is calculated in the same way as the curve for the flat-fading channel. With this method multiple channel realizations are generated each time. The channel realization with the highest power will be used for calculating the PER of that time instant. In our scenarios only two channel realizations are needed, but this can be extended. The expected diversity order can be calculated with Equation 3.31. The diversity order L is equal to the number of transmission channel realizations (see Tse and Viswanath [27, p. 62]).

Figure 3.9 shows the performance of selection diversity method in a single input multiple output (SIMO) flat-fading channel. There are several curves, which show the performance of different scenario. The first two curves are obtained with Monte-Carlo simulation, with approximation of AWGN performance (Q-function). The third curve is obtained with Monte-Carlo simulations with a floating-point IEEE 802.11a model. The last curve is calculated with equation 3.31, were ($L = 2$).

3.4.3 Delay diversity

Delay diversity is a combination of frequency and spatial diversity. In a flat-fading channel with or without selection diversity the final channel response remains flat. This means that COFDM modulation does not gain anything from frequency selectivity of the channel. In short, all the carriers have the same amount of SNR, which depends on the channel coefficient h_n.

We now introduce a delay element in one of the receiver branches; this will give a frequency selective channel response. The delay element is chosen to be larger than the sample time ($T_s = 50ns$). When using delay diversity, it requires only a single delay element without any control. Therefore the name poor-mans MIMO. Figure 3.8 shows the block-diagram of this method.

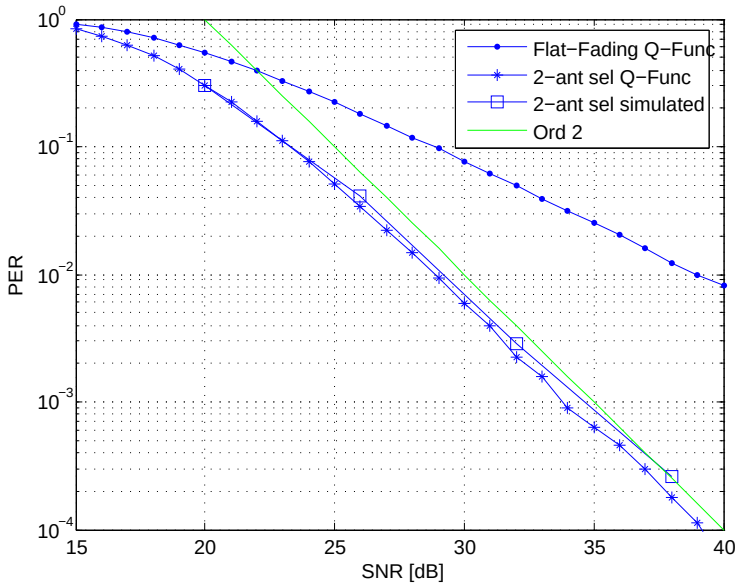

Figure 3.9: Performance of SIMO selection diversity for 54Mbit/s.

$$r(t) = \sum_{n=0}^{N-1} h_n s(t-\tau_n) + n_n(t). \tag{3.34}$$

Equation 3.34 shows the general description of delay diversity. In this equation N is the number of transmission channels. In the RT-CV a maximum of 4 transmission channels could be created. The scenario which is defined in Subsection 3.1.3 on page 3.1.3, $N = 2$, $\tau_0 = 100ns$ and $\tau_1 = 0ns$. We assume that the moduli of channel coefficients (h_n) have a Rayleigh distributions, and that they are uncorrelated.

The Fourier transform of this channel is given in Equation 3.35. This channel response will be cyclic, depending on the $\tau = \tau_0 - \tau_1$. If we want to gain from delay diversity, at least one cycle must be in the bandwidth of an IEEE 802.11a signal, i.e $\tau > 1/B$.

$$h(t) = h_0\delta(t) + h_1\delta(t - tau_1). \tag{3.35}$$
$$H(\omega) = h_0 + h_1 e^{\jmath\tau_1\omega}. \tag{3.36}$$

With this method the channel response will be frequency-selective. Figure 3.10 shows an example channel realization of this method. Inside the bandwidth of IEEE 802.11a OFDM symbol the channel is not flat, but frequency selective. For this method the antenna channel responses are assumed to be uncorrelated. By placing the antennas far away from each other, this can be realized.

Figure 3.11 depicts the PER curves of the different scenarios. These results come from Monte-Carlo simulations with a floating-point simulation of the IEEE 802.11a simulation model. The

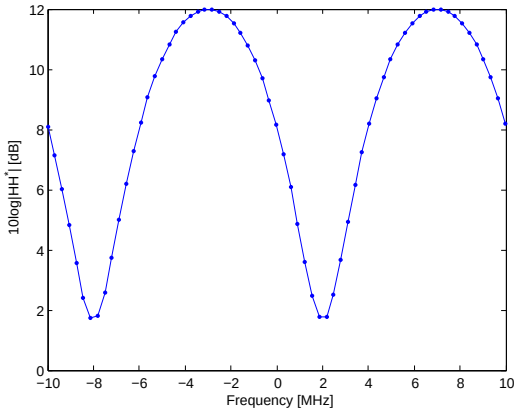

Figure 3.10: Delay diversity channel response.

simulation of the delay-diversity curve is based on two receive antennas with a delay difference of 100ns. For a detailed analysis, see van Houtum [31].

As conclusion of the delay diversity method, the diversity order (slope) remains the same as selection diversity, but in our simulation model it turns out to 1dB worse. This method is a blind method, which explains the difference between both the methods. This diversity-technique can relatively simply be applied to the transmitter, but also it could be used in the receiver. One disadvantage is that creating delay elements on frequency of 5.xGHz is not that easy. These elements are not yet available, therefore in the RT-CV we created a delay on IF frequency.

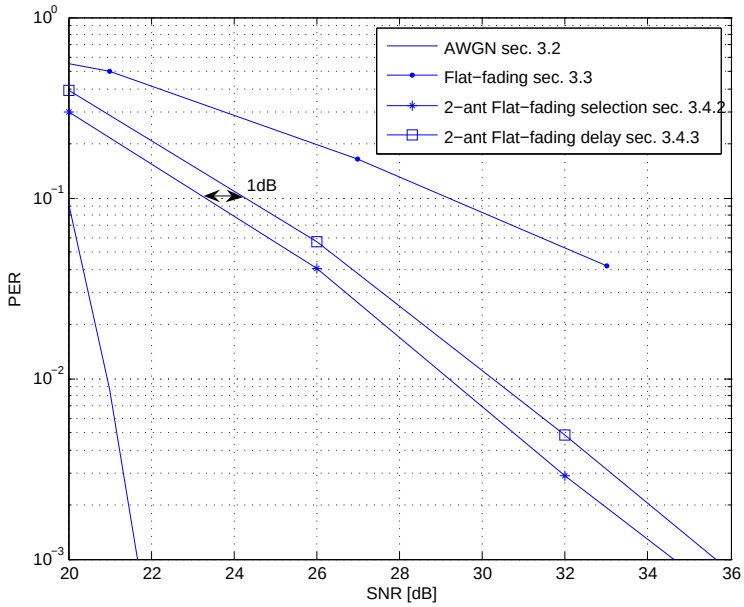

Figure 3.11: Floating-point simulation results for all the scenarios for 54Mbit/s.

Chapter 4

Receiver Validation

In this chapter the measurement results, based on the Tahoe chip will be presented. This chapter will contain an introduction. This section will go in more details in measurements, which were done while design the real-time concept validator (RT-CV) and measurements that are needed for testing. The second section will contain a detailed description of the receiver architecture. The third section will be a discussion about the performance of the analog digital (AD) converters and low pass filter (LPF). The last part will go in more details in the overall performance of the Tahoe chip for different scenarios.

4.1 Introduction

Figure 4.1 shows a block diagram of the RT-CV. There are two data-paths, one is the transmitter, the other the receiver. The data-source of the transmitter is an MPEG streamer PC, which generates a bit stream. The next block is the mini-MAC, this is an field programmable gate array (FPGA), which contains a simple medium access control (MAC). In this block, the MPEG packets will be re-packed into IEEE 802.11a packets. These packets will be translated into a complex-baseband signal in the base-band transmitter. The radio will modulate this signal to a 5.x GHz signal. The receiver will demodulate and decode the received signal in a bit-stream, which can be decoded by the MPEG decoder.

The usual method of testing such a system is evaluating each block individually. In this section there will be a rough evaluation, which will be refined in the next sections. The first hypothesis can be done based on measurements, which are done while designing the RT-CV.

In the design of RT-CV end-to-end tests are done. This means that for example the complex base-band signal from the transmitter will be coupled to the receiver. These tests will check if there are no functional errors in the system. This will not give any indication of the performance of the system.

The performance of the Transmitter is tested with the vector signal analyzer (VSA). This measurement instrument is an off-line reference receiver, which can demodulate the complex base-band or radio frequency (RF) signal and gives an indication of the quality of the signal in terms of error vector magnitude (EVM). The quality of the transmitter signal is sufficient enough (EVM $\approx -38dB$).

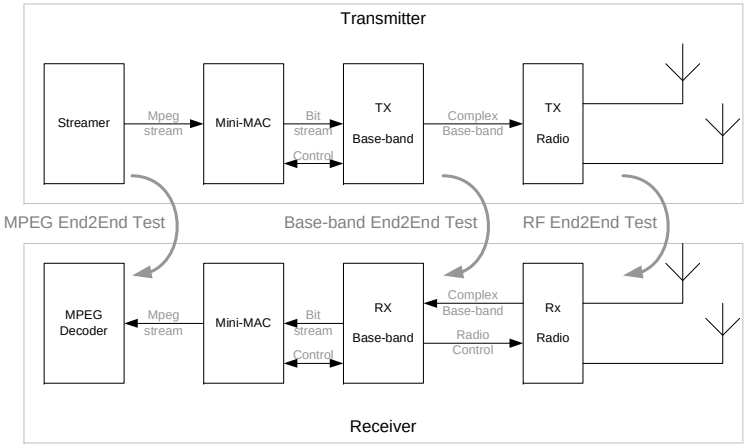

Figure 4.1: Block diagram of RT-CV.

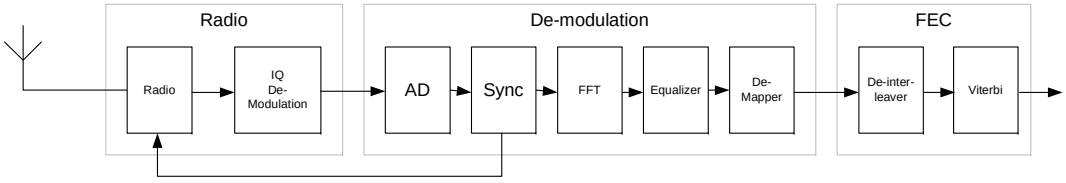

Figure 4.2: Block diagram of receiver.

From the measurements with the VSA and the end-to-end tests, it is clear that the transmitter has got an acceptable performance. This means that the receiver is causing the problems.

4.2 Implemented Receiver

This section will discuss the receiver, which is implemented in the Tahoe and the RT-CV. Figure 4.2 shows the receiver block diagram in more detail. This diagram does not contain the mini-MAC and MPEG decoder. The radio of the receiver is tested with VSA and the performance degradation is acceptable. This means that this part will not be discussed in this thesis. This section will discuss more about receiver base-band processing. This part needs to demodulate a complex base-band signal into bits.

As commonly used measurement method for evaluating such a system, is first evaluating the first block in the system, then the second and so on. This measurement method involves, that we can capture the data after each block. The data must be processes off-line to be sure what the performance is of each individual block. We start with evaluating the AD converter and so on. Due to technical limitations of the system only the AD converter could be tested separately.

The input of the base-band processor will be used as reference point for signal to noise ratio (SNR). The first block is the AD converter. This block is intergraded in the Tahoe chip. The first measurements are done on the performance of this AD converter. (see Section 4.3 on page 37).

The second block of the base-band processor is the synchronization unit. This unit contains a feedback to the radio, which controls the gain steps in the radio. This automatic gain control (AGC) loop is partly discussed in Subsection 3.1.1 on page 20. The other two functions of this block is frequency and time recovery. In the measurements that are done in Section 4.4 on page 43 the frequency recovery and AGC algorithms are disabled, only the time estimation is used.

The third block is the fast Fourier transform (FFT), which will demodulate the time-domain samples in frequency domain components or sub-carriers. The FFT is an implementation of the discrete Fourier transform (DFT) operation. For more information about the FFT operation see Enden [28, 172-173].

The next block in the receiver base-band processor is the equalizer, which has two functions. The first function is the common phase error (CPE) correction. This correction will be discussed in Appendix C on page 85. The other function of the equalizer is a compensation of the channel response. In the Tahoe a zero forcing (ZF) equalizer is implemented. In Chapter 5 on page 49 there will be a detailed description of this algorithm.

The de-mapper will decode the output of the equalizer in a bit-metrics. A bit-metrics gives the probability that a bit has a certain value. For the calculation of the bit-metrics the channel state information (CSI) is needed. The output of the Tahoe equalizer does not have this information any more. The equalizer generates a second signal, which indicates the CSI for each sub-carrier. The de-mapper will also be discussed in Chapter 5 on page 49.

The de-interleaver will re-order the bit-metrics. This operation is the inversion of the interleaver (see Section 2.2.1 on page 15). This operation is included to spread unreliable bit-metrics, due to fading, within an OFDM-symbol. Otherwise these unreliable bit-metrics will remains together, which will cause block errors.

The Viterbi algorithm will try to correct the bit errors. This is done based on the bit-metrics, which is calculated in the de-mapper. These metrics contain information how reliable a certain bit is. The Viterbi algorithm can correct bit errors, because there is redundancy in the signal.

4.3 Performance of AD Convertor

In this section we will discuss the measurements, which are done to characterize the performance of the AD converter. The implemented AD converter contains two analog inputs. (in-phase (I) signal and quadrature (Q) signal). This converter needs to have an acceptable performance. The first subsection will be a description of the measurement setup. The following subsections will go into more details about the measurement and the results of these measurements.

4.3.1 Measurement setup

In this subsection there will be a description of the measurement setup, which is used for measuring the performance of the AD converter. Figure 4.3 shows a block diagram of the measurement setup for these tests.

The measurement setup contains a PC, which utilizes a digital analog (DA) converter card that has a better performance as the AD converter. In this measurement setup the performance of the AD converter will be dominant. The analog signal from the PC is filtered with analog LPF. This

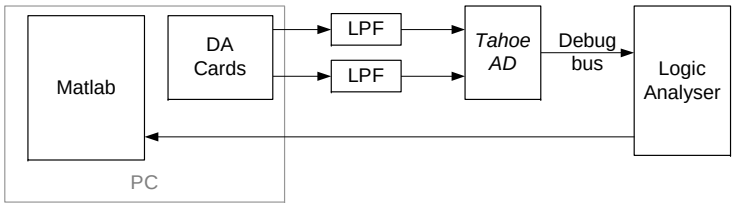

Figure 4.3: Measurement setup for measuring the performance of the AD convertor.

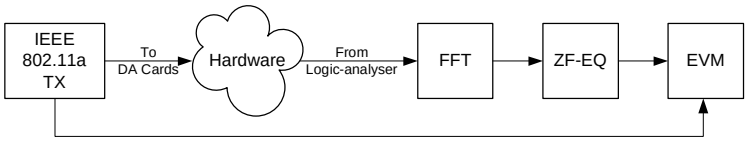

Figure 4.4: Block-diagram of the Matlab code.

filter will remove the higher order aliases. The AD digital output will be captured with a logic analyzer. The data of this measurement device will be analyzed in the PC with Matlab.

Figure 4.4 shows a detailed block diagram of the Matlab code. The Matlab code contains an IEEE 802.11a transmitter, which is the floating-point equivalent of the implemented Tahoe transmitter. The signals from the AD converter (logic-analyzer) will be processed in Matlab. The logic-analyzer will be triggered from the transmitter. This means that the Matlab code knows the timing of the transmitted signal. The FFT transforms the time-domain samples in a frequency domain signal. The output of the FFT will be equalized with a ZF equalizer. This equalized signal will be used to calculate the EVM. There is a direct relation between EVM and SNR; this relation will be discussed in details in Appendix A on page 77.

The Matlab receiver will calculate an EVM value for different timing offsets. This EVM value is calculated over a sufficient number of orthogonal frequency division multiplexing (OFDM)-symbols and frames, as defined in the standard [25, p. 30]. This will give an curve were the EVM will be large if the timing is in-correct due to inter symbol interference (ISI), otherwise there will be no ISI, but the actual performance of the AD converter. (see figure 4.5).

The maximum performance of the AD converter can be simulated. From the data sheet of the integrated AD converter an effective number of bits (ENOB) of 8.7 is specified. With this number, an approximation of the expected EVM could be calculated. Equation 4.1 shows the maximum SNR. It is known from van Nee [32, Ch. 6], that OFDM modulation requires a back-off around 10dB. From van Houtum [30], it is clear that is 1.7dB performance degradation, due to

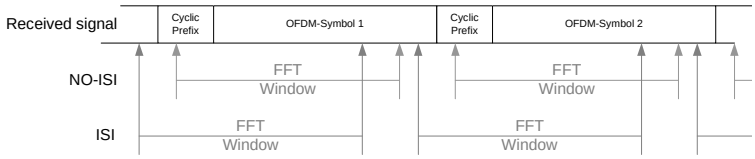

Figure 4.5: Inter symbol interference in OFDM system.

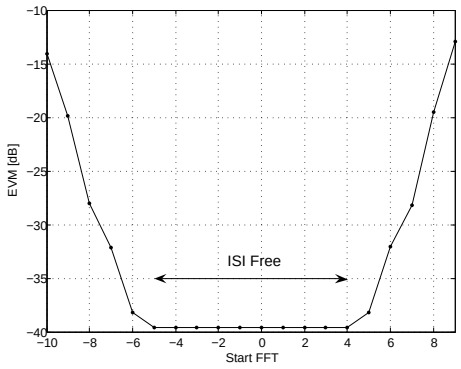

Figure 4.6: Simulated expected performance of the AD converter.

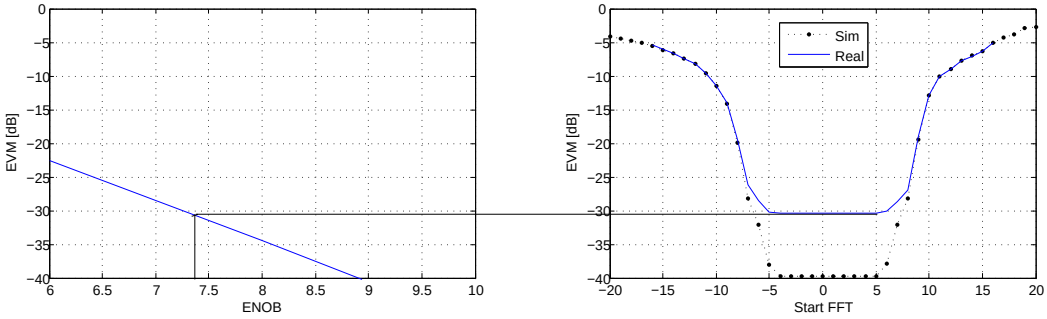

Figure 4.7: Performance AD converter of Tahoe.

equalization. (see Appendix A on page 77).

$$SNR_{max} = 6n_{ENOB} = 52dB EVM = -SNR_{max} + 10 + 1.7 \approx 40dB \tag{4.1}$$

If we model the AD converter and simulate the performance of this AD converter. Figure 4.6 depicts the results of the simulation. This curve contains an ISI free region of 10 samples. The cyclic prefix of the IEEE 802.11a system is 16 samples, which was expected to be the number samples of the ISI free region. The different between the measured region and the expected region is caused by the sample rate converter (SRC), which is implemented in the transmitter. This SRC contains a finite impulse response (FIR) filter this fades the OFDM-symbol transitions. The curve is not symmetric because the cyclic prefix has got an even number of samples.

4.3.2 Performance of Tahoe AD converter

The measured performance of the Tahoe AD converter is depicted in Figure 4.7. The right plot shows the performance of the AD converter with different time offsets. The performance of the AD converter degrades, if the time-offset is too large due to ISI. The left plot contains a calculation of the performance in EVM for different ENOB.

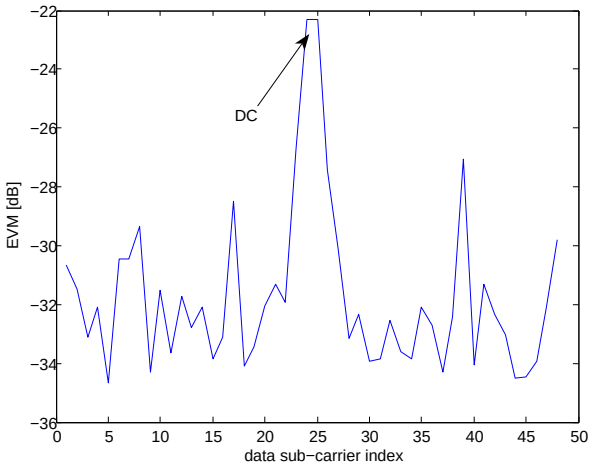

Figure 4.8: Performance AD converter of Tahoe, EVM spectrum.

From this measurement it is clear, that the performance of the Tahoe AD converter in terms of ENOB is around 7.4 bits. There is a difference in expected performance and measured performance of roughly 1.4 bits. This performance degradation could be caused by IQ-imbalance. Appendix B on page 81, there is a discussion about this sort of mismatches. The first mismatch, which could appear is gain mismatch. In this measurement the gain error of the AD converter is calibrated with test tones.

Figure 4.8 shows the EVM spectrum of the Tahoe AD converter. This figure shows the EVM per data subcarrier. The sub-carrier with the lowest index is the most negative data sub-carrier. The highest index shows the most positive sub-carrier. The zero padding, DC and Pilot carriers are not in this figure. If there was a delay mismatch in the AD converter, the EVM spectrum should not be flat, but decrease for higher frequencies. Figure B.2 on page 84 shows this effect in terms of signal to interference ratio (SIR).

One may derive from Figure 4.8 that the AC coupling, which is used in the analog data-path of the AD, is not well designed. Otherwise the carriers around DC (subcarrier 24/25) would have the same performance as all the others. Other conclusions could not be made on these measurements. There could also be other effects, which influence the performance of the AD converter such as clock-jitter, cross-talk, decoupling of power supplies or harmonic distortion. These effects will not be discussed in this thesis.

4.3.3 Performance of external AD converter

An external AD converter is applied to the system. This converter is connected to the Tahoe chip on the debug bus. This converter was needed to achieve better performance. If we observe the data-sheet of this converter, it could have an ENOB of more then 10 bits. If we calculate the expected SNR on the same way we did in the previous section, the EVM could be somewere around -48dB.

If we measure the performance with the same method as we did for the Tahoe AD converter, then the performance of this converter is better (see Figure 4.9), but still not good enough. Figure

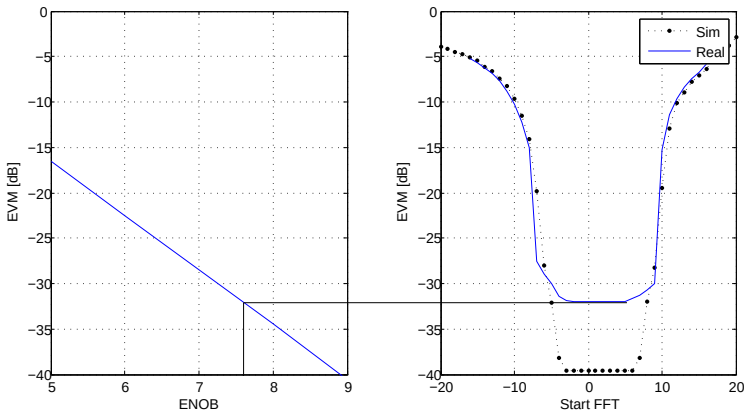

Figure 4.9: Performance external AD converter.

4.10 shows the EVM spectrum of the external AD converter, this is not flat any more. This effect can be caused by the fact that there is delay or phase mismatch.

As mentioned before, if there is a delay mismatch, then the performance of the system improves, if a delay is applied. In the hardware a delay to one of the two analog signals could be applied. Figure 4.11 shows the performance of the system with different delays. A positive number means that the I signal is a number of nanoseconds later as the Q signal.

If we apply -1ns delay we get the best performance. The performance (-40dB) is not the expected performance of this AD converter. The performance is in the same order, as we expect from the Tahoe AD. The last remark of this measurement is the method to obtain the expected EVM, which is calculated in Equation 4.1, is not very accurate. There were differences of more the 8dB, between the expected EVM and measured EVM. This means that the value of ENOB is not accurate measure for obtaining the expected performance in terms of EVM.

4.3.4 Measurement of the LPF

This last part of this section are measurements, which are performed with the LPF alone. The absolute delay or phase of the LPF could be measured with s-parameter measurement set. This measurement instrument can characterize any analog component, not only in terms of gain but also in terms of phase. From the phase-shift a delay can be calculated. Figure 4.12 shows at the left side the absolute phase and delay of the filters. The discontinuity in this plot is mainly because of the measurement instrument and not the low-pass filters. The right plots show the difference in terms of phase and delay between both of the filters. This difference causes a part of the performance degradation of the external AD converters.

We can calculate the final performance of this LPF on these measurement results. The calculations of phase error, which are done in Appendix B on page 81 are used to calculate the SIR. The performance is shown in Figure 4.13, were at the left side, there is the performance of the low-pass filters with no compensation and the other curve shows the performance with 1ns delay. This delay is created by adding a coax cable of sufficient length to one of the branches. If we compare this figure with the performance in Figure 4.10 then they are in the same order

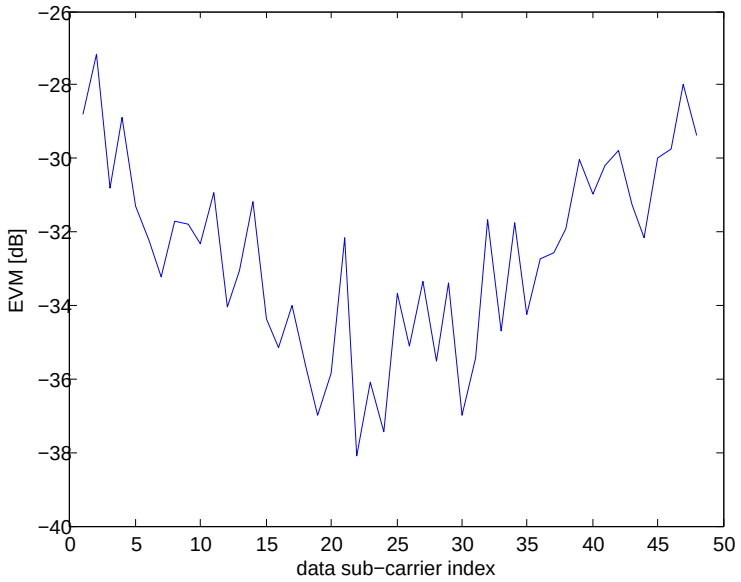

Figure 4.10: Performance external AD converter.

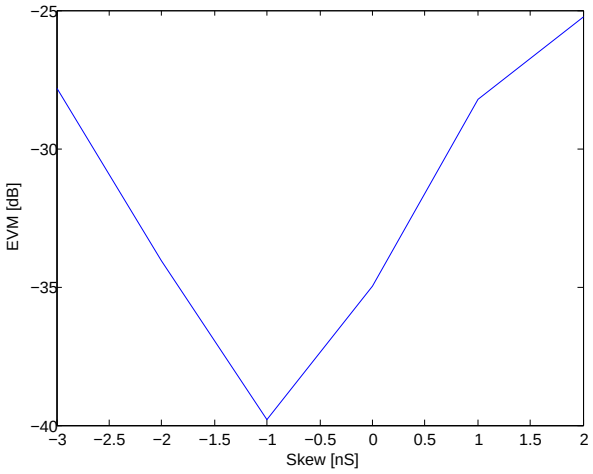

Figure 4.11: Performance external AD converter in terms of different values of IQ skew.

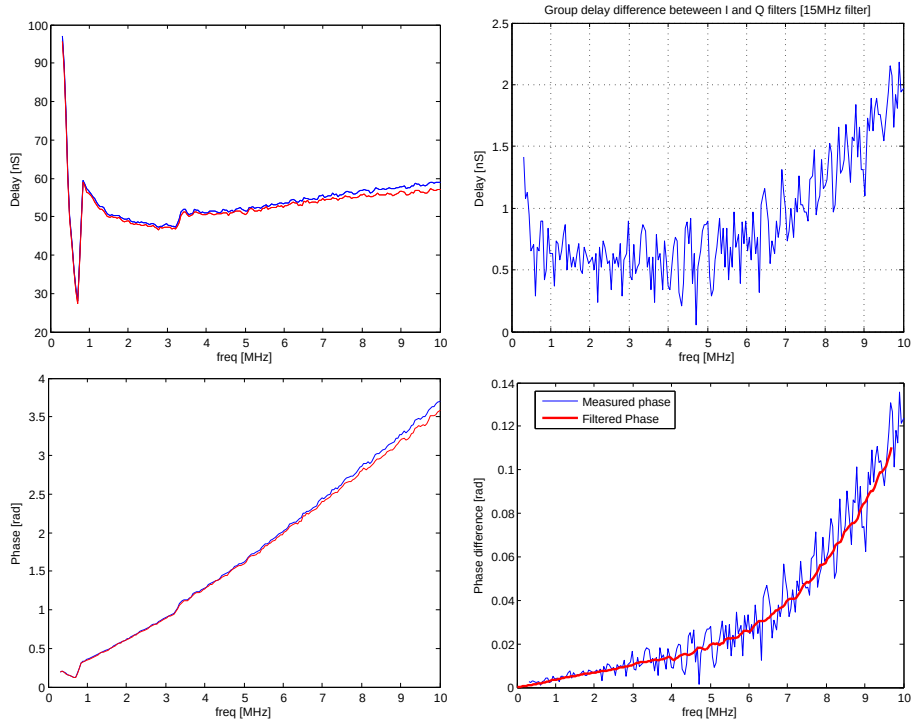

Figure 4.12: Delay and Phase of the low-pass filters.

($EVM = -SNR + 1.7dB$) for the high-frequency sub-carriers. The minimum and maximum frequency of IEEE 802.11a OFDM signal is around 8MHz.

4.4 Overall Receiver Performance Measurements

The following measurement is the performance test of the synchronization unit in the Tahoe, but due to technical problems all the other blocks in the receiver could not be tested individually. This means that the whole receiver chain has to be tested at once. This measurement will obtain the PER for different scenarios, described in the Subsection 3.1.3 on page 25.

This section contains two parts. The first subsection will be a description of the measurement setup. The second subsection will show the results of these measurements.

4.4.1 System measurement setup

In Figure 4.14, there is the block diagram of the measurement setup. This measurement setup contains a PC, which is used to test the Tahoe receiver. This PC generates in Matlab test vectors for the measurement setup.

The Matlab code contains a floating-point IEEE 802.11a transmitter. This transmitter will generate a 40MHz complex base-band signal. There is a channel model, which applies channel model and add noise to the signal. This model is an equivalent complex base-band channel model, which

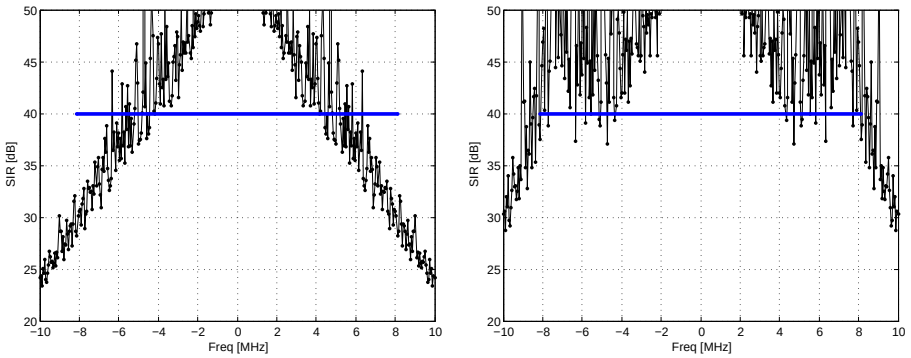

Figure 4.13: Performance without and with compensation.

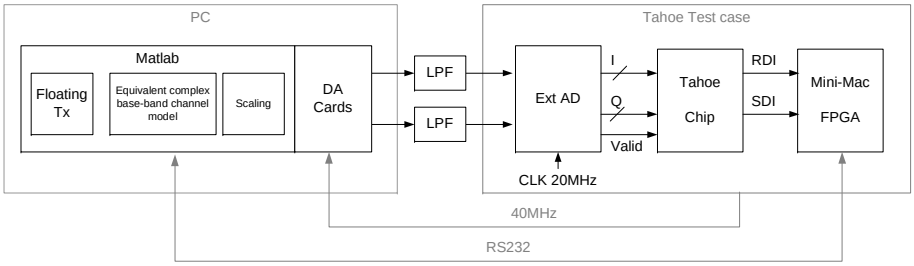

Figure 4.14: System performance measurement setup.

contains all the scenarios, which are described in subsection 3.1.3 on page 25. The last part of the Matlab code is the scaler, this will scale the output of the channel model, in such a way that the DA would not clip. This block will replace the AGC in the receiver. In normal operation the received power of the base-band processor will be held constant with AGC. In this setup there is no AGC present, so the input power of the AD converter will be scaled, with the scaling block in the Matlab code.

The LPF is added to suppress the aliases form the analog signal. This signal will be converted to the digital domain with an external AD. This digital signal is transferred to the Tahoe chip, which demodulates the signal.

In this measurement setup the DA and AD clocks are locked. This means that the 40MHz clock of the DA converter and the 20MHz clock of the AD are generated form the same crystal. This means, that there is no drift between both of the sample clocks. If the clocks are locked the sample clock error can be ignored.

The Tahoe will automatically de-modulate the complex base-band signal. The received data will be transferred to the mini-MAC. This is a FPGA, which contains a simple MAC protocol. For this measurement two communication busses are used. One interface is for the received data (the RDI) and the other for control of the chip (the SCI). These interfaces could not communicate directly to the PC. The mini-MAC will calculate for each received frame a CRC word. This CRC word will be compared in Matlab with the transmitted CRC. The Matlab code will account the number of packets and errors.

The Matlab code is scheduled as follows. It sends a frame, then it will wait until a CRC is received

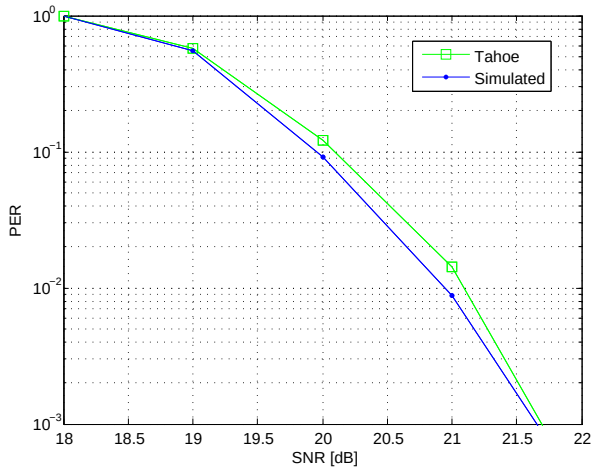

Figure 4.15: Measured performance of AWGN channel for 54Mbit/s.

on the RS-232 port. After that it will be checked. If there is no CRC received, then this frame is also count as erroneous. There are a few cases, were no CRC is generated. The first case is that the synchronization did not detect any frame. The second case is, that the signal field is decoded incorrect. This will give the receiver wrong information. In the signal field there is a parity bit to check if the signal field is corrupt or not.

4.4.2 PER measurement results

These measurements will follow the test scenarios, as described in Subsection 3.1.3 on page 25. The first measurements are based on a single input single output (SISO) system with additive white Gaussian noise (AWGN) channel. Figure 4.15 shows the performance, which is both measured and simulated (see section 3.2 on page 26). The difference between these curves is very small, as expected. In this scenario the channel response at baseband is not frequency selective.

The second scenario is done with SISO system in a flat-fading channel. The channel response in this scenario is still flat. Figure 4.16 depicts the measured and simulated results of this scenario. This means that the Tahoe chip still performs good compared to the simulated performance.

The third scenario is done with selection diversity. The receiver makes a selection between two receive antennas (SIMO system). The channel responses of the both signals are uncorrelated. The channel response of this method remains flat. The Tahoe performs still as expected form simulations.

The last scenario is done with delay diversity. A 100ns delay is applied to one of the receiver branches. Figure 4.18 shows the performance of the Tahoe and expected simulation results. It is clear that the performance is not as expected. Compared to the SISO flat-fading simulation there is a gain. This gain comes from the fact, that there are multiple receive antennas. This diversity method will introduce frequency selectivity in the signal (see Figure 3.10 on page 33). The Tahoe has to equalize the signal in terms of magnitude.

As a hypothesis two receiver blocks could cause this performance degradation. The first block is the synchronization unit. This unit still performance time synchronization. This algorithm is

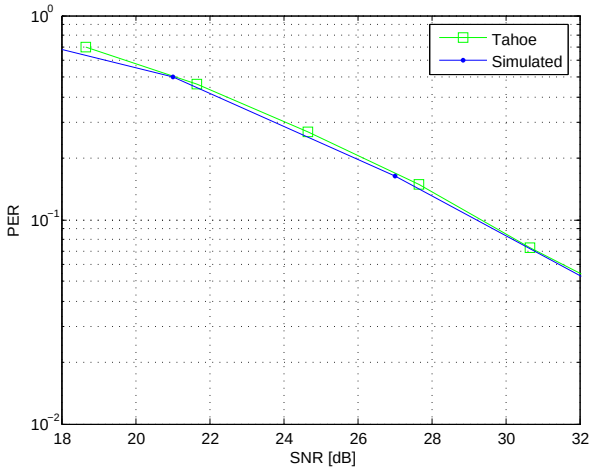

Figure 4.16: Measured performance of SISO flat-fading channel for 54Mbit/s.

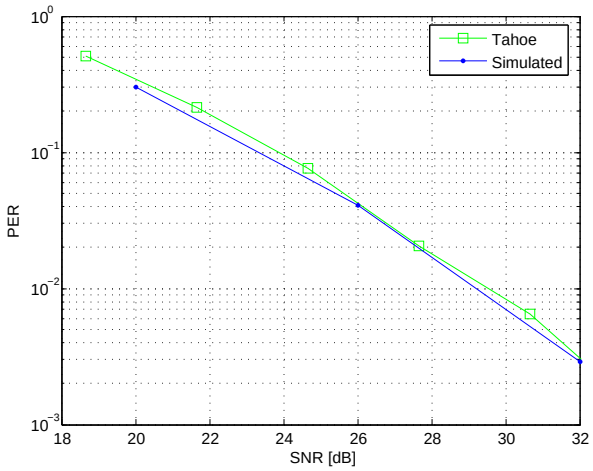

Figure 4.17: Measured performance of SIMO selection diversity for 54Mbit/s.

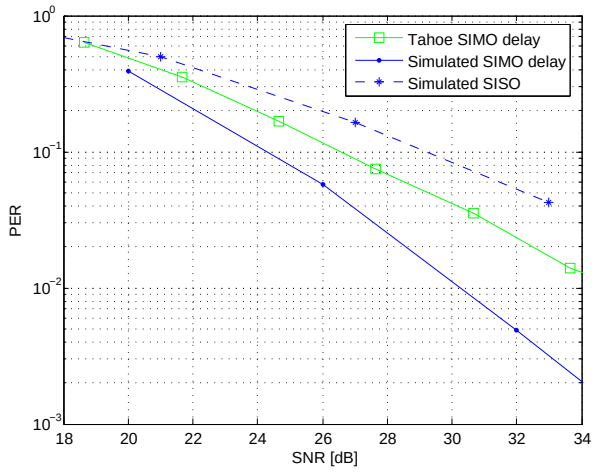

Figure 4.18: Measured performance of SIMO delay diversity for 54Mbit/s.

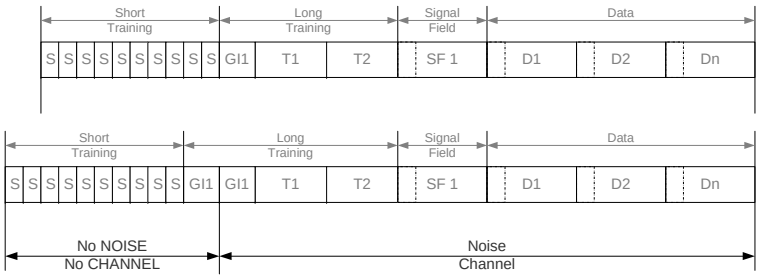

Figure 4.19: Modified IEEE 802.11a framing structure.

expected to have no influence on this measurement. The performance of the Tahoe is again measured, but with a modified framing structure. Figure 4.19 shows this new framing structure, were on the first part of the preamble no noise and channel is applied. This means that the time synchronization is perfect.

Figure 4.20 shows the difference, between the normal synchronization and the perfect synchronization. The differences between those measurements are very limited. This means that the synchronization has no influence on the final performance.

The other algorithm, which could cause the performance degradation, is the equalizer. The equalizer clips (exceed finite number representation) in these measurements, what can checked by hand. If there is a packet error, the clipping of the equalizer will be observed. This observation gives an interesting result, that around 1 out of 10 errors the equalizer not clipped for a SNR of 34dB. As we observe the packet error rate (PER) curve in Figure 4.20 at 34dB and take one tenth of the measured PER, it will come exactly on the expected curve. Therefore as hypothesis the equalizer is causing the performance degradation. The next chapter will go in more details about this algorithm

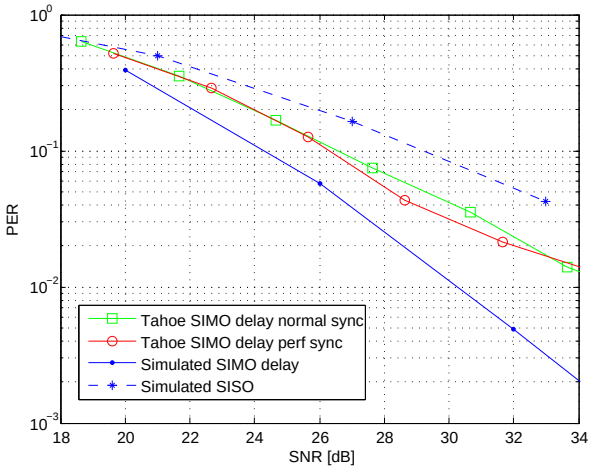

Figure 4.20: Different between perfect sync and normal sync.

Chapter 5

Equalizer and De-mapper

This chapter contains a detailed description of the equalizer and the de-mapper algorithms. These blocks are situated after the fast Fourier transform (FFT)-block in the receiver (see Figure 4.2 on page 36). The main task of the equalizer is to do the channel correction. The standard method of equalization is zero forcing (ZF) equalization and this is also applied in the Tahoe chip. minimal mean square error (MMSE) equalization is a different technique. In this chapter both methods will be compared.

The first section of this chapter contains simulation results. These simulations are needed to compare the implemented equalizer in the Tahoe chip to a floating-point equalizer in software. This is done to show that the Tahoe equalizer is causing performance degradation. The second section consists of a description of two different equalization methods. The third section contains a description of the implementation of the Tahoe equalizer. The last section contains a proposal for new equalizer algorithms.

5.1 Simulations with Tahoe and Floating-point Equalizer

In Chapter 4 on page 35 we have presented measurement results for the Tahoe chip. A hypothesis based on these results is, that the equalizer part of the Tahoe is causing performance degradation. To prove this, a Matlab simulation is done. The simulation will compare the results of the Tahoe equalizer, with that of the floating-point equalizer.

The Matlab model of the implemented equalizer is very slow, because it is a bit- and cycle-true model, therefore a pragmatic solution is used. Both of the equalizers get the same signals. This simulation is done for one signal to noise ratio (SNR) of 34dB and only for the delay-diversity scenario.

Figure 5.1 depicts the block diagram of the simulation model. The transmitter generates a frequency domain signal. The channel model will modify this signal. The tuner will scale (AGC) the OFDM symbols in such away that it is in the operation point of the Tahoe equalizer. This equalizer is a fix-point model, which means that the input has a finite number representation. If the input signal magnitude is incorrect the performance of the equalizer degrades.

The signals are equalized and decoded, both by the Tahoe equalizer and the floating-point model. Table 5.1 contains the results of this simulation. As a result of this simulation it is clear that the

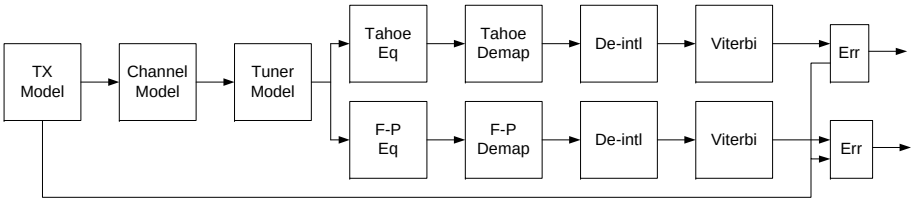

Figure 5.1: Block diagram of the comparison Matlab model.

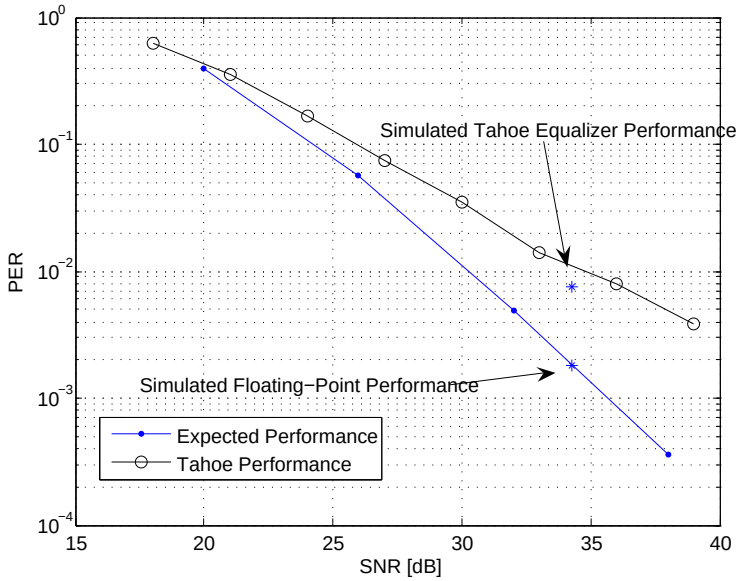

Figure 5.2: PER curve in the case of Delay Diversity.

Equalizer	SNR	Number Test	Errors	PER
Floating-Point	34	10000	76	7.6e-2
Tahoe	34	10000	16	1.6e-2

Table 5.1: Error comparison between Tahoe and Floating-point equalizer.

floating-point model generates 16 packet errors, while the Tahoe equalizer generates 76 packet errors. These results can be found in Figure 5.2. This figure contains the results from simulation from Section 3.4.3 on page 31. The other curve is the Tahoe measurement result from Figure 4.18 on page 47. From the figure it clear that the floating-point equalizer has the same packet error rate (PER) as expected. This result is obvious, because both of the simulation models are the equivalent. The Tahoe equalizer has a PER, which is worse than expected.

From this simulation, it is clear that the performance of the Tahoe equalizer is dominant, in the contribution of the measured performance degradations. Therefore there will be a more detailed description, about the equalizer algorithms in this chapter.

5.2 Equalizers Algorithms

In this section, ZF and MMSE equalizer will be discussed. In Proakis [21, p. 601-617], these equalizers are discussed more in theory. In this system the channel response is estimated based on long training symbols. This estimation can be improved by updating the estimation based on the received signal (adaptive decision feedback equalization).

The equations of the two equalizer algorithms are:

- ZF equalizer : $\hat{S}_k = \frac{(H_k S_k + N_k)}{\hat{H}_k}$.
- MMSE equalizer : $\hat{S}_k = \frac{\hat{H}_k^*(H_k S_k + N_k)}{\hat{H}_k \hat{H}_k^* + \hat{\sigma}^2}$.

This equation shows is the calculation for the k-th sub-carrier. The S_k is the transmitted symbol and $\hat{S}_k$ is estimate. H_k is the channel response and $\hat{H}_k$ is the estimated channel response. N_k is the added white noise and variable σ^2 is the noise power.

5.2.1 Zero forcing equalizer

In Proakis [21, sec. 10.2], there is a detailed description of the ZF equalizer. Equation 5.2 is the calculation of coefficient C_k, for a ZF equalizer. The received signal is multiplied with this coefficient. This will give an estimation of the transmitted symbol $\hat{S}_k$. In this context a symbol is the data, which is on a sub-carrier and is modulated base on BPSK, QPSK or QAM modulation. Each orthogonal frequency division multiplexing (OFDM) symbol contains 48 of these symbols.

$$\hat{S}_k \quad = \quad C_k R_k = C_k(H_k S_k + N_k), \tag{5.1}$$

$$C_k = \frac{1}{\hat{H}_k}, \tag{5.2}$$

$$\hat{S}_k = S_k + \frac{N_k}{H_k}. \tag{5.3}$$

In this section, we will simplify the problem and assume that the estimated channel transfer coefficient is exactly the same as the real channel transfer coefficient ($\hat{H}_k = H_k$). Equation 5.3 is the resulting signal. The power of the noise term now depends on the channel response. The noise will be amplified, if the magnitude of the channel response is small.

One benefit of this algorithm is, that the output of the equalizer contains the same constellation that is transmitted, only with noise added to it. This means that the output of this equalizer can directly be used for calculating the error vector magnitude (EVM) (see Appendix A on page 77). In case of additive white Gaussian noise (AWGN) channel the calculated EVM has got a direct relation with the added noise.

5.2.2 MMSE equalizer

For more details about the MMSE equalizer can be found in Proakis [21, sec. 10.2]. This equalizer will multiply the received signal R_k with coefficient C_k. The output of the equalizer is the estimated symbol $\hat{S}_k$. The MMSE equalizer will minimize the average error, between the send symbol S_k and the estimated symbol $\hat{S}_k$ (see equation 5.5). From Proakis [21, sec. 10-2], it is clear that the coefficient C_k has to be Equation 5.6.

$$\hat{S}_k = C_k R_k = C_k(H_k S_k + N_k) \tag{5.4}$$

$$\min(E|\varepsilon_k|^2) = \min(E|S_k - \hat{S}_k|^2) \tag{5.5}$$

$$C_k = \frac{\hat{H}_k^*}{\hat{H}_k \hat{H}_k^* + \hat{\sigma}^2} \tag{5.6}$$

In figure 5.3, there is a comparison between the coefficient C_k for a ZF equalizer and an MMSE equalizer. In this plot we assume that the $\sigma^2 = 0.01$. This means that there is behavior transition at -20 dB channel response. From this figure, it is clear that for small magnitudes of the channel response the noise will not be amplified with MMSE. The transition point of the equalizer depends on the σ^2.

One advantage of the MMSE equalizer is, that the dynamic range of the coefficient C_k is limited. This property is nice for fixed-point implementations. Figure 5.4 shows the output of both the equalizers. From this figure it is clear that the dynamic range of the MMSE equalizer is less than that of the ZF equalizer, see the outliers in the left figure. This is also a good property of the MMSE equalizer, for a fixed-point implementation. If the noise power is very small or the channel coefficient is very large, this equalizer will acts as a ZF equalizer (large SNR).

5.2.3 Noise estimation

The main disadvantage of the MMSE equalizer is that it needs the noise power σ^2. The receiver has no information about the noise power however. In Tahoe there is no algorithm available, that

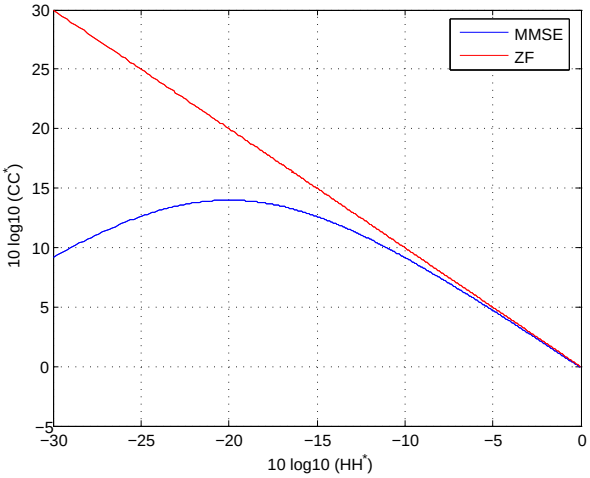

Figure 5.3: Comparison of coefficient C_k for the ZF and MMSE equalizer.

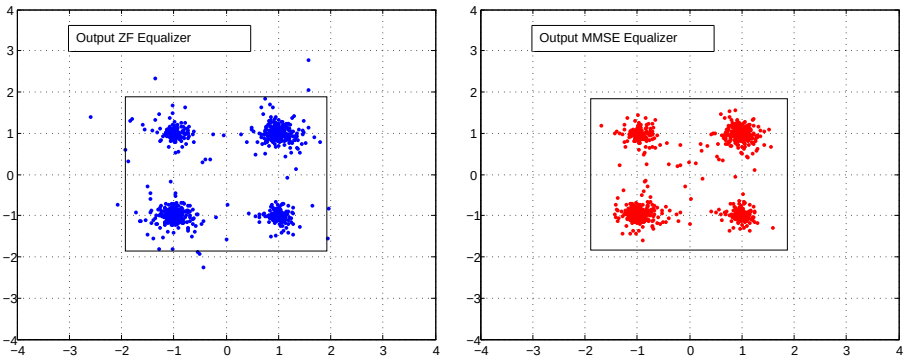

Figure 5.4: Constellation of both the equalizers at 20dB SNR.

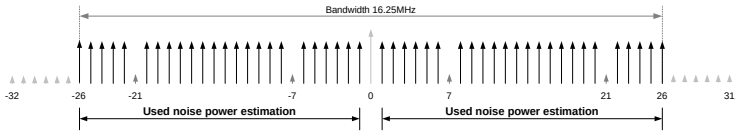

Figure 5.5: Used sub-carriers for noise variance estimation.

can estimate the noise power. In the implementation the noise power could be estimated on the basis of the power detector in the automatic gain control (AGC) (see Figure 3.4 on page 23). There is a direct relation between the SNR and input signal power. For this estimation the noise figure of the radio must be known in the base-band processor.

In this section a new noise estimation algorithm will be presented. This algorithm relies on the fact, that there are two OFDM training symbols in the long training sequences. These two symbols are identical and can be used for two purposes.

The first purpose, which is implemented in the Tahoe chip, is to get a better estimate of the channel response. Equation 5.8 shows this method, were $R1_k$ is the received first training sequence and $R2_k$ the second received training sequence. There is a common term $H_k S_k$ in this equation. If we add both signals, the magnitude of the desired signal is amplified by a factor of 2 and the magnitude of the noise with $\sqrt{2}$.

$$\hat{H}_k = \frac{R1_k + R2_k}{S_k} = \frac{(H_k S_k + N1_k) + (H_k S_k + N2_k)}{S_k} \tag{5.7}$$

$$\hat{H}_k = \frac{2H_k S_k + \sqrt{2}N_k}{S_k} = 2H_k + \frac{\sqrt{2}N_k}{S_k} \tag{5.8}$$

The second purpose is noise power estimation (or variance). Subtracting the two training symbols we can do this. The noise will remain in the difference-signal. Both of the noise terms $N1_k$ and $N2_k$ are uncorrelated. This signal can be used to estimate the noise power (see equation 5.11).

$$N_k = R1_k - R2_k = (H_k S_k + N1_k) - (H_k S_k + N2_k) = N1_k - N2_k, \tag{5.9}$$

$$\hat{\sigma}^2 = \frac{1/52 \sum_{k=0}^{51} (N_k N_k^*)}{2}, \tag{5.10}$$

$$\hat{\sigma}^2 = \frac{1/52 \sum_{k=0}^{51} (R1_k - R2_k)(R1_k - R2_k)^*}{2}. \tag{5.11}$$

This estimation is based on the data sub-carriers and pilots of the OFDM symbol, and thus on the relevant bandwidth (see figure 5.5). The DC sub-carrier will not be used in this estimation. This sub-carrier contains the DC offset, which has no correlation with the noise. The zero sub-carriers are not used in this estimation, because the transition bands of low-pass filters in the radio will start on these frequencies.

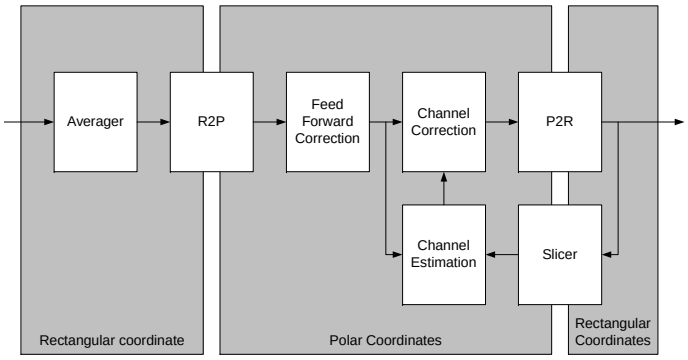

Figure 5.6: Tahoe equalizer block-diagram.

5.3 Tahoe Implementation

This section will give a description of the Tahoe implementation. This will be done in two subsections. The first subsection consists of the implemented equalizer and the second about the implemented de-mapper algorithm.

5.3.1 Implemented equalizer

Figure 5.6 depicts the block diagram of the implemented equalizer structure of the Tahoe chip. Most of the blocks in the equalizer are using polar coordinates for writing complex numbers. This method gives some implementation benefits. E.g. to do a multiplication of two complex numbers in hardware, 4 real multiplications in rectangular coordinates are needed. The same operation in polar coordinates can be done by doing one addition (of the phase) and one multiplication (for the magnitude).

The first block is the averager. This algorithm will average the two OFDM symbols of the long training sequence. This algorithm is less complex in rectangular coordinates than in polar coordinates. Equation 5.12 shows the equation of the averager. This algorithm uses in hardware two additions (I and Q) and a shift operation (./2).

$$R(k) \quad = \quad \frac{R1(k) + R2(k)}{2}. \tag{5.12}$$

The second block is the rectangular to polar coordinate converter. This is done with the cordic algorithm; this implies that the gain of this block is 0.8234 (see Hu [15]). This algorithm estimates the phase and magnitude of a rectangular complex signal in an iterative way.

The third block is the feed forward correction (FFC); this block will do the common phase error (CPE) estimation and correction. There will be a CPE due to remaining frequency error in the signal. This frequency error can be caused by phase noise or remaining frequency errors. The CPE will be estimated based on the pilots. This correction will be done in the frequency domain in a feed-forward loop. This correction will be discussed in Appendix C on page 85.

The channel estimation (CHest) block compares the received long training sequence to the transmitted long training sequence. Based on that comparison the channel response can be estimated (see equation 2.4 on page 18). The output of the CHest is the inverse of the channel response. This is used as correction of the data, which is done by the channel correction (CHC). There is feedback from the slicer. This means that based on the output of the equalizer the estimated channel response will be updated. This feedback loop is disabled in the measurements.

$$C_k = \frac{1}{\hat{H}_k}, \tag{5.13}$$

$$\arg(C_k) = -\arg(\hat{H}_k), \tag{5.14}$$

$$|C_k| = \frac{1}{|\hat{H}_k|}. \tag{5.15}$$

In the CHest the inverse of the channel response is calculated. This channel inversion in terms of the phase can be perfectly calculated in a finite number representation (see equation 5.14). The major problem is the calculation of the magnitude ($\frac{1}{|\hat{H}_k|}$). For very small values of the magnitude of the estimated channel response ($\hat{H}_k$), the output of the CHest will be very large (see equation 5.15). Therefore this value is limited in the CHest in finite number representation. This effect is called clipping.

$$\hat{S}_k = C_k \cdot R_k, \tag{5.16}$$

$$\arg(\hat{S}_k) = \arg(C_k) + \arg(R_k), \tag{5.17}$$

$$|\hat{S}_k| = |C_k||R_k|. \tag{5.18}$$

The CHC performs a multiplication of the C_k with the received signal R_k. The output magnitude of the $|\hat{S}_k|$ could also be clipped, due to finite number representation (see Equation 5.17). The last part of the equalizer is the polar to rectangular coordinate conversion. In this converter the signal could also be clipped. In different blocks and algorithms in the equalizer the signal could be clipped. This means that the clipping errors propagate through the equalizer.

This equalizer will remove channel state information (CSI) from the signal. This can be observed from Equation 5.3, were the term of $|H_k|$ disappeared from the output signal. This CSI is needed for reliable forward error correction (FEC) however. Therefore the CSI is calculated in a separate signal in the equalizer. This CSI signal indicates the relative channel magnitude. Equation 5.19 is the Tahoe implementation of the CSI signal.

$$CSI_k = \frac{|H_k|}{(1/48)\sum_{n=0}^{48}|\hat{H}_k|} \tag{5.19}$$

$$CSI_k = \frac{1}{|C_k|(1/48)\sum_{n=0}^{48}|\hat{H}_k|} \tag{5.20}$$

The calculation of the CSI signal is based on the data from the CHest (see Equation 5.20). This data could be clipped; this means that the CSI could be based on corrupted data. A conclusion is that equalizing may sometimes result in clipped operations. This clipping is a non-linear operation, which will lead to un-predictable effects in the equalizer.

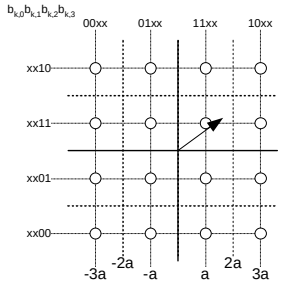

Figure 5.7: A 16-QAM constellation.

5.3.2 Implemented de-mapper

The de-mapper transforms the signal from the equalizer into bits. The de-mapper must make decisions based on the output vector of the equalizer. There are two possible methods; the first method is called hard-decision and the second one is called soft-decision de-mapping. In soft-decision de-mapping the de-mapper provides also the reliability information of the bits.

In this part we will take 16-QAM signals as an example. Figure 5.7 depicts the constellation diagram of this modulation method. Note that Gray-mapping is applied. There are several decision boundaries parallel to the real and imaginary axis.

The hard-decision bit-metrics for 16-QAM can be calculated with equation 5.21. In these equations a $+1$ represent a logical one and a -1 represent a logical zero. For the example output vector from the equalizer in Figure 5.7 the output of the de-mapper will be "1111".

$$\begin{aligned}
\hat{b}_{k,0} &= sign\left(\Re\left(\hat{S}_k\right)\right), \\
\hat{b}_{k,1} &= -sign\left(\hat{b}_{k,0}\Re\left(\hat{S}_k\right) - 2a\right), \\
\hat{b}_{k,2} &= sign\left(\Im\left(\hat{S}_k\right)\right), \\
\hat{b}_{k,3} &= -sign\left(\hat{b}_{k,2}\Im\left(\hat{S}_k\right) - 2a\right).
\end{aligned} \tag{5.21}$$

If we assume that our modulation method is M-QAM there will be m bits ($M = 2^m$) and p bits per axis (in-phase and quadrature) ($m = 2p$). The hard-decisions equations for M-QAM modulation and Gray-mapping are now:

$$\left.\begin{aligned}
X_0 &= \Re(\hat{S}_k) \\
\hat{b}_{k,i} &= sign(X_i) \\
X_{i+1} &= -(\hat{b}_{k,i}X_i - a2^{p-i-1}).
\end{aligned}\right\} \quad i = 0..p-1 \tag{5.22}$$

$$\left.\begin{aligned}
Y_0 &= \Im(\hat{S}_k) \\
\hat{b}_{k,i+p} &= sign(Y_i) \\
Y_{i+1} &= -(\hat{b}_{k,i+p}Y_i - a2^{p-i-1}).
\end{aligned}\right\} \quad i = 0..p-1 \tag{5.23}$$

These equations hold for the bit mapping, which is defined in the standard [25, p. 20]. It is clear that BPSK modulation is an exception, because $p = 1/2$ there. For this modulation type only the first real received component is used.

For better system performance soft-decision de-mapping must be used. The paper of Goff [9] is used as reference. If we consider two orthogonal signals X_k and Y_k, which represent the in-phase and quadrature signals in the receiver:

$$X_k = \alpha_k A_k + I_k, \tag{5.24}$$
$$Y_k = \alpha_k B_k + Q_k. \tag{5.25}$$
$$\tag{5.26}$$

In this equation α_k is the magnitude of the channel response $|H_k|$ and this is Rayleigh distributed. The signal A_k contains the real part of the transmitted symbol and B_k the imaginary part of the transmitted symbol. The noise is I_k and Q_k, these two signals are uncorrelated.

$$A_k = \Re(S_k), \qquad I_k = \Re(N_k), \tag{5.27}$$
$$B_k = \Im(S_k), \qquad Q_k = \Im(N_k). \tag{5.28}$$

The log-likelihood ratio (LLR) for each of the m bits is defined by:

$$\Lambda(b_{k,i}) = \ln\left(\frac{P_r\{b_{k,i} = 1/X_k, Y_k\}}{P_r\{b_{k,i} = 0/X_k, Y_k\}}\right) \qquad i = 0..m. \tag{5.29}$$

The following equation gives the exact LLR for the first p bits:

$$\Lambda(b_{k,i}) = \ln\left(\frac{\sum_{i=0}^{2^{p-1}-1} \exp\left\{-\frac{(X_k - \alpha_k a_{1,i})^2}{2\sigma^2}\right\}}{\sum_{i=0}^{2^{p-1}-1} \exp\left\{-\frac{(X_k - \alpha_k a_{0,i})^2}{2\sigma^2}\right\}}\right) \quad i = 0..p-1 \tag{5.30}$$

In this equation $a_{1,i}$ and $a_{0,i}$ respectively represent the realization of symbols A_k conditionally on $b_{k,i} = 1$ and $b_{k,i} = 0$. If we assume a binary phase shift keying (BPSK) modulation, with constellation point a for a logical one and $-a$ for a logical zero, the LLR can be calculated:

$$\begin{aligned}\Lambda(b_{k,0}) &= \ln\left(\tfrac{p\{X_k|A_k\}}{p\{X_k|-A_k\}}\right) \\ &= \ln\left(\frac{\exp\left(-\frac{(X_k - a\alpha_k)^2}{2\sigma^2}\right)}{\exp\left(-\frac{(X_k + a\alpha_k)^2}{2\sigma^2}\right)}\right) \\ &= \tfrac{2a}{\sigma^2} X_k \alpha_k.\end{aligned} \tag{5.31}$$

Each bit-metric will be multiplied with a constant $c = \frac{2a}{\sigma^2}$. It is important to observe that the value of this constant has no effect on the maximization process within the Viterbi-decoder. Therefore we can ignore this constant (set it to one).

$$\begin{aligned}\hat{\Lambda}(b_{k,0}) = \quad & X_k\alpha_k \\ & = (\alpha_k A_k + I_k)\alpha_k \\ & \approx \Re(\hat{S}_k)|\hat{H}_k|^2\end{aligned} \tag{5.32}$$

In this equation, $\hat{S}_k$ is the output of the equalizer and $|\hat{H}_k|^2$ is the CSI, which is required for correct calculation of the LLR. The calculations that are needed to calculate the LLR for 16QAM and 64-QAM are complicated to implement in hardware. Therefore in the Tahoe chip a linear approximation of LLR is used. This approximation is also proposed in Goff [9, p. 647] and van Houtum [30]. A good approximation of the LLR can be achieved using the following expressions:

$$\begin{aligned}\hat{\Lambda}(b_{k,0}) &= X_k/\alpha_k, \\ \hat{\Lambda}(b_{k,i}) &= |\hat{\Lambda}(b_{k,i-1})| - a2^{p-i}, \quad i = 1..p-1, \\ \tilde{\Lambda}(b_{k,i}) &= c\alpha_k^2\hat{\Lambda}(b_{k,i}), \qquad\quad i = 0..p-1.\end{aligned} \tag{5.33}$$

and:

$$\begin{aligned}\hat{\Lambda}(b_{k,p}) &= Y_k/\alpha_k, \\ \hat{\Lambda}(b_{k,i+p}) &= |\hat{\Lambda}(b_{k,i-1+p})| - a2^{p-i}, \quad i = 1..p-1, \\ \tilde{\Lambda}(b_{k,i+p}) &= c\alpha_k^2\hat{\Lambda}(b_{k,i+p}), \qquad\quad i = 0..p-1.\end{aligned} \tag{5.34}$$

Signals X_k/α_k and Y_k/α_k can be approximated by the output signals of the equalizer.

$$X_k/\alpha_k \approx \Re\hat{s}_k, \tag{5.35}$$

$$Y_k/\alpha_k \approx \Im\hat{s}_k. \tag{5.36}$$

The CSI in this case is:

$$\alpha_k^2 \approx \tilde{H}_k\tilde{H}_k^*. \tag{5.37}$$

$\hat{\Lambda}(b_{k,i})$ is the linear approximation of the LLR without CSI, were $\tilde{\Lambda}(b_{k,i})$ is the approximation with CSI. Variable a is a constant which indicates the magnitude of the constellation (see Figure example in 5.7 for 16-QAM).

The bit-metrics $\tilde{\Lambda}$ are quantized with 4-bits (16-levels). In Rahnema [22], this number is shown to be sufficient enough. The constant c in the equations 5.33 and 5.34 is variable, that scales quantization levels of the soft-decision de-mapper. This variable can be set in the software of the Tahoe. There is more information about quantization in Heller [14].

From Equations 5.33 and 5.34, the correct CSI value from the equalizer consists of factor $|H_k|^2$. In the implementation this value consists only the factor $|H_k|$ (see equation 5.20). This is one of the errors in the implementation of the Tahoe. This effect error is investigated and this apparently does not cause major performance degradation (see van Houtum [29]).

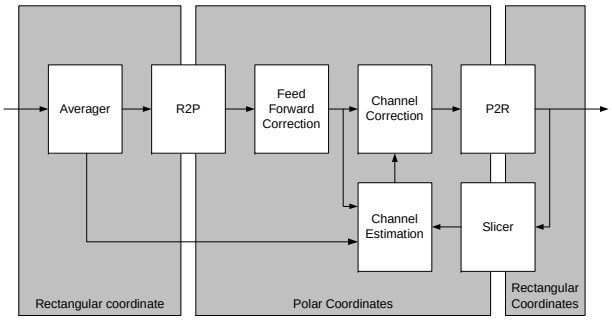

Figure 5.8: Block diagram MMSE implementation equalizer structure.

5.4 Proposed Equalizer and De-mapper

In this section we will describe two equalizer-proposals, which can be implemented. The first proposal is an implementation of an MMSE equalizer, which will not need a lot of changes in the current design of the Tahoe equalizer. The second proposal is a division-less equalizer algorithm. Both of these proposals will be discussed in this section.

5.4.1 Implementation of MMSE equalizer

With some modifications in the current equalizer, an MMSE equalizer could be implemented. The extra hardware what is needed is very limited. For this proposal, we use the same equalizer structure as implemented in Tahoe, which is in block diagram of Figure 5.8. In this subsection only the blocks, which need to be modified will be discussed.

The averager averages the training symbols, but noise variance estimation must be added to this block. The algorithm, that needs to be implemented, is in Equation 5.11 on page 54. This method substraction sub-carriers from each other and averages this over the number of sub-carriers.

The CHest in the implementation is calculating the inversion of the channel response $1/\hat{H}_k$, but this need to be changed in an MMSE coefficient, which is in equation 5.38. The value of $\hat{\sigma}^2$ is estimated in the averager.

$$C_k = \frac{\hat{H}_k^*}{\hat{H}_k \hat{H}_k^* + \hat{\sigma}^2}. \tag{5.38}$$

$$\tag{5.39}$$

The phase of this coefficient can calculated with the following expression:

$$\arg(C_k) = -\arg(\hat{H}_k). \tag{5.40}$$

$$\tag{5.41}$$

The magnitude of this coefficient is:

$$|C_k| = \frac{|\hat{H}_k|}{|\hat{H}_k|^2 + \hat{\sigma}^2} \tag{5.42}$$

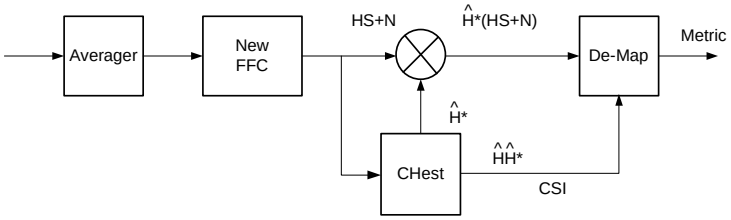

Figure 5.9: The proposed equalizer structure.

(5.43)

The CSI calculation is based on a relative number which is in equation 5.44.

$$CSI_k = \frac{48\hat{H}_k\hat{H}_k^*}{\sum_{n=0}^{48-1}\hat{H}_n\hat{H}_n^*}. \tag{5.44}$$

5.4.2 Implementation of division-less equalizer and de-mapper

The previous proposal does nor require many changes in the current Tahoe implementation. The second proposal requires more modifications but need less processing power. This method is called division-less decoding. In this section this new proposal will be discussed. Figure 5.9 depicts the block diagram of this new structure.

This proposed new structure will not do a division in the equalizer, but a multiplication instead. This means that the output signal of this equalizer still contains the CSI (see equation 5.45). This information is needed for proper calculation of the LLR.

$$C_kR_k = \hat{H}_k^*R_k = \hat{H}_k^*(H_kS_k + N_k) = \hat{H}_k^*H_kS_k + \hat{H}_k^*N_k. \tag{5.45}$$

It is clear that the output of the equalizer is biassed with a factor of $H_kH_k^*$. The de-mapping can be achieved by taking this biasing in account, using the following expressions:

$$\begin{aligned} \hat{\Lambda}(b_{k,0}) &= c\cdot\Re(\hat{H}_k^*R_k), \\ \hat{\Lambda}(b_{k,i}) &= |\hat{\Lambda}(b_{k,i-1})| - a\cdot\hat{H}_k\hat{H}_k^*\cdot 2^{p-i}, \quad i = 1..p-1, \end{aligned} \tag{5.46}$$

and

$$\begin{aligned} \hat{\Lambda}(b_{k,p}) &= c\cdot\Im(\hat{H}_k^*R_k), \\ \hat{\Lambda}(b_{k,i+p}) &= |\hat{\Lambda}(b_{k,i-1+p})| - a\cdot\hat{H}_k\hat{H}_k^*\cdot 2^{p-i}, \quad i = 1..p-1. \end{aligned} \tag{5.47}$$

In this equations variable a is the magnitude of the constellation, which is defined in Figure 5.7. The bit-metrics $\hat{\Lambda}$ need to be quantized in a 4-bit representation. The constant c is used to set the quantization levels on correct value.

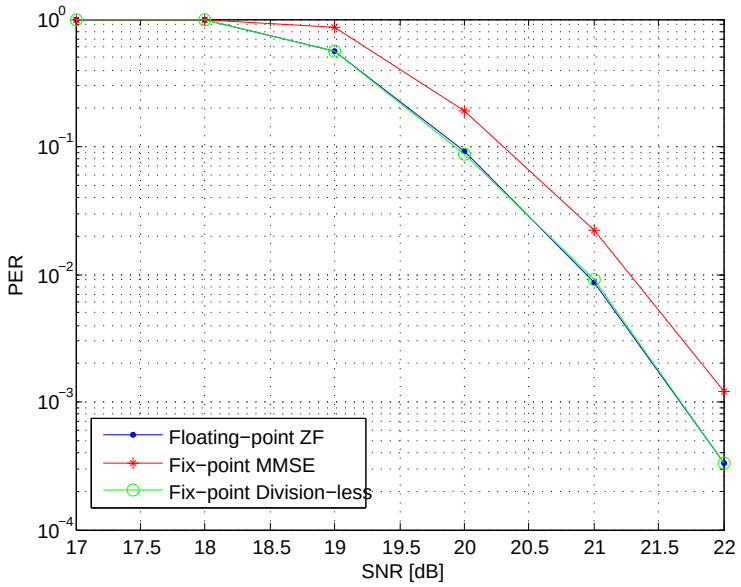

Figure 5.10: Performance of proposed new structures for an AWGN channel for 54MBit/s.

5.4.3 Simulation results of proposed algorithms

Simulations are done, to demonstrate that these proposed algorithms have a good performance. The algorithms are converted to fix-point models, which could be directly implemented in hardware. The block diagram of this simulation is the same as in Figure 5.1 on page 50. Now there are three equalizers in parallel. The first equalizer is the floating-point zero-forcing equalizer; this equalizer can be used as reference model for the others.

The simulations are done with the different scenarios, which are defined in Subsection 3.1.3 on page 25. The first simulation is the performance of the three equalizers for an AWGN channel. The results are in Figure 5.10. The first curve is the performance of a floating-point zero-forcing equalizer. The second curve is the performance of the MMSE equalizer. This equalizer give a small performance degradation. This can be caused by the fix-point implementation, but also the non-linear compensation (see Figure 5.3). This non-linearity is not compensated in the de-mapper. The last curve contains the performance of the division-less equalizer, which does not show any performance degradation compared to the floating-point equalizer.

The same effect could be obtained from the simulation results for flat-fading without diversity (see Figure 5.11), with selection diversity (see Figure 5.12) and delay diversity (see Figure 5.13). The conclusion from these simulations is that the fixed-point division-less algorithm does not produce any noticeable performance degradation compared to the floating-point equalizer. The MMSE equalizer is suffering a little bit in performance.

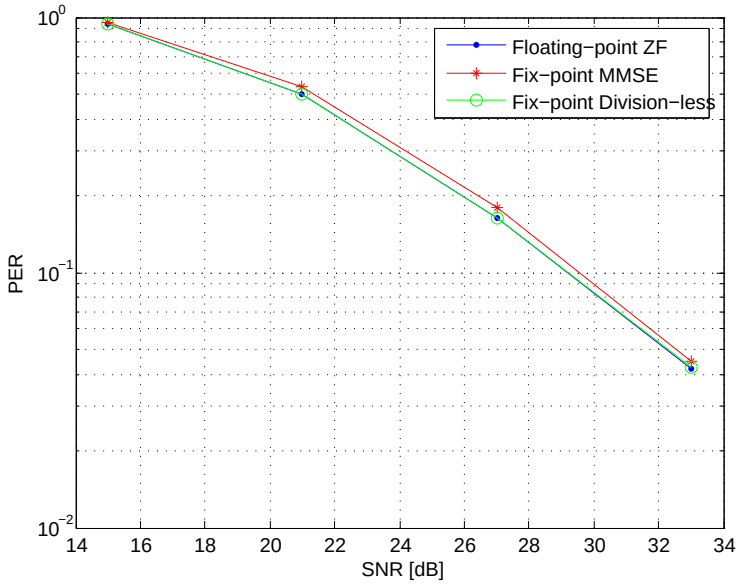

Figure 5.11: Performance proposed new structures flat-fading for 54MBit/s.

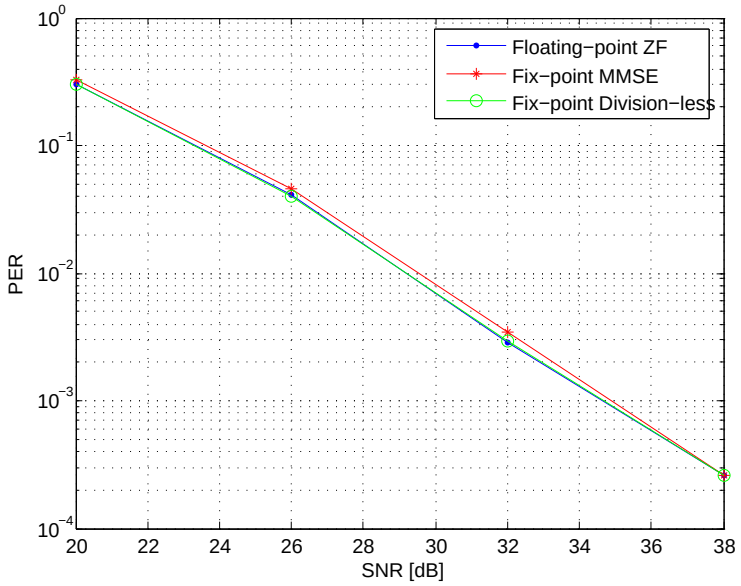

Figure 5.12: Performance proposed new structures selection diversity for 54MBit/s.

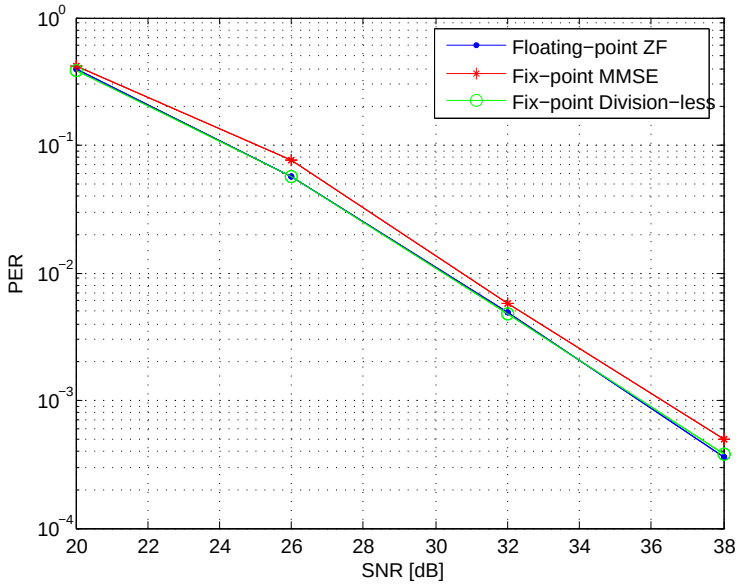

Figure 5.13: Performance proposed new structures delay diversity for 54MBit/s.

Chapter 6

Conclusions and Recommendation

The concept of delay-diversity for an in home environment is considered to be an elegant method for creating diversity in WLANs. This method can be implemented at low complexity in the transmitter or receiver, if there are appropriate delay elements available. The delay-diversity method however did not show any performance gain on the real-time concept validator (RT-CV) that was developed at Philips Research. The first objective of this thesis was therefore to show why this RT-CV did not exhibit any performance gain. A second objective was to propose modifications to the RT-CV so that it does demonstrate the advantage of delay diversity.

6.1 Conclusions

Regarding the work performed in this thesis, the following conclusions could be drawn:

- The performance of the embedded analog digital (AD)-converter was not good. The influence of this AD-converter on the total performance of the system could be significant. Why the AD-converter is not performing well has not been investigated. It is possible that the performance degraded due to AC coupling of the AD-converter, but also cross talk, clock jitter, design of printed circuit board (PCB) or something else could cause the degradation.

- An external AD-converter was used for testing the performance of the Tahoe base-band processor. The quality of this external AD-converter was essentially better than that of the embedded converter, however now phase mismatches appeared. To overcome this problem the signal in one of the demodulator branches was delayed. This resulted in an acceptable performance.

- The expected system performance of the Tahoe chip was determined (by measurements) for the AWGN channel, a flat-fading (Gaussian noise) channel without diversity (single-input and single-output) and with selection diversity (single-input and two outputs). The actual performance of the Tahoe chip for delay-diversity did not meet the expected performance.

- Measurements indicated that the synchronization-units in the Tahoe do not cause any noticeable performance degradation.

- From measurements of the Tahoe chip we could conclude that its equalizer is clipping in the case of delay-diversity. We could not observe any clipping effects in the other scenarios. This observation resulted in the hypothesis that the equalizing method could cause the performance degradation. Simulations, confirmed this hypothesis.
- In the Tahoe chip a zero forcing (ZF) equalizer is implemented. This equalizer structure does not perform well in fixed-point setting. Therefore other equalizer structures would be preferable. In Chapter 5 there are two proposals for new equalizer implementations. The simulations with these newly proposed equalizer implementations, did not show any unacceptable performance degradations. These algorithms could not be directly implemented in the current RT-CV however.

6.2 Recommendations

It is clear from this thesis that a new equalizer implementation is necessary. Since this is impossible to implement in the current RT-CV, a new base-band processor has to be developed,e.g. in a field programmable gate array (FPGA) or digital signal processor (DSP). If the base-band processor is programmable, new algorithms can be prototyped in a real-time environment. A second option is to use an other existing base-band processor.

The second recommendation is to study the synchronization methods in more depth. From the measurements it was clear that the algorithm in the Tahoe chip shows no noticeable performance degradation. These measurements were done at 54Mbit/s however, which implies that the SNR was relatively large. It is unclear whether the synchronization algorithms in the Tahoe also perform well at smaller SNR. This requires further attention.

The IQ-mismatch-measurements could only be carried out with high-quality (and expensive) equipment. The final design of a wireless local area network (WLAN) system must therefore contain algorithms that reduce IQ-mismatch, since these mismatches can lead to a dramatic decrease of performance.

The proposed equalizer algorithms were developed for an IEEE 802.11a system. It would be a good idea to study these algorithms also in a MIMO setting. Maybe these methods could be applied in new IEEE 802.11n base-band processors.

Acknowledgments

This Master Thesis would be incomplete without thanking those people who helped me to make it possible. I would also like to thank all the people who support me while doing my study.

First of all I would like to thank my supervisors, Frans Willems and Wim van Houtum. I would also like to thank everybody helping me writing this document: Frans Willems, Ronald Rietman, Arie Koppelaar and Paul Vranken. I would like to thank Jean-Paul Linnartz and Stephan Borgers given me the opportunity to do my master Thesis project within Philips Research. I would also like to thank Jan Bergmans, for his contribution to this project.

I would like to thank all the guys from Philips: Peter Rutten, Paul van Voorthuisen, Eric Penning de Vries, Job Oostveen, Maurice Stassen and Stan Baggen.

Last of all I would like to thank my family and friends: Joke, Noa and Ru.

Luc Tan
Eindhoven, April 2006

References

[1] Netgear rangemax product sheet. http://www.netgear.com/products/details/WPN824.php.

[2] Vlsi technolgy datasheet vsc10ad01. 0.20-Micron VSC10AD01 10 Bit A/D Converter -Rev. 0.2.

[3] V. Abhayawardhana and I. Wassell. Common phase error correction with feedback for ofdm in wireless communication. In *Global Telecommunications Conference GLOBECOM 2002*, volume 1, pages 651–655. IEEE, Nov 2002.

[4] S. Alamouti. A simple transmit diversity technique for wireless communications. *IEEE Journal on Selected Areas in Communications*, 16(8):1451–1458, Oct 1998.

[5] N. Chayat. Tentative criteria for comparison of modulation methods. *Doc. IEEE 802.11-97/96*, Sept. 1997.

[6] D. Devasirvatham. Multi-frequency propagation measurements and models in a large metropolitan commercial building for personal communications. *IEEE PIMRC'91*, Conference Proceedings 1991.

[7] D. Devasirvatham, M. Krain, D. Rappaport, and C. Banerjee. Radio propagation measurements at 850 mhz, 1.7 ghz and 4 ghz inside two dissimilar office building. *Electronics Letters*, 26(7):445–447, March 1990.

[8] E. Dilling. Equalizer study for wireless multimedia: algorithms, structure and performance. Technical report, Philips Semiconductors SLE, 2000.

[9] S. L. Goff, A. Glavieux, and C. Berrou. Turbo-codes and high spectral efficiency modulation. In *in Proc. International Conference on Communications*, pages 645–649, 1994.

[10] P. Hafezi, D. Wedge, M. Beach, and M. Lawton. Propagation measurements at 5.2 ghz in commercial and domestic environments. *IEEE PIMRC'97*, Conference Proceedings 1997.

[11] H. Hashemi. The indoor radio propagation channel. *Proceedings of the IEEE*, 81(7):943–968, Jul. 1994.

[12] D. A. Hawbaker and T. S. Rappaport. Indoor wideband radiowave propagation measurements at 1.3 ghz and 4.0 ghz. *Electronics Letters*, 26(21):1800–1802, Oct. 1990.

[13] S. Haykin and M. Moher. *Modern Wireless Communications*. Prentice Hall, 2005.

[14] J. Heller and I. Jacobs. Viterbi decoding for satellite and space communication. *IEEE Transactions on Communications*, 19(5):835–548, Oct 1971.

[15] Y. H. Hu. Cordic-based vlsi architectures for digital signal processing. *IEEE Signal processing Magazine*, 9(3):16–35, July 1992.

[16] P. Nobles and F. Halsall. Delay spread and received power measurements within a building at 2 ghz, 5 hz and 17 ghz. In *In Proceedings 10th International Conference on Antennas and Propagation*, volume 2, pages 319–324, April 1997.

[17] B. O'Hara and A. Petrick. *The IEEE 802.11 handbook; a designer's companion*. IEEE, 1999.

[18] R. Parot and F. Harris. Resolving and correcting gain and phase mismatch in transmitters and receivers for wideband ofdm systems. In *Conference Record of the Thirty-Sixth Asilomar Conference on Signals, Systems and Computers*, volume 2, pages 1005–1009, Nov 2002.

[19] D. Petrovic, W. Rave, and G. Fettweis. Common phase error correction with feedback for ofdm in wireless communication. In *15th IEEE International Symposium on Personal, Indoor and Mobile Radio Communications*, volume 3, pages 1901–1905. IEEE, Sept 2004.

[20] L. Piazzo and P. Mandarini. Analysis of phase noise effects in ofdm modems. *IEEE Transactions on Communications*, 50(10):1696–1705, Oct 2002.

[21] J. Proakis. *Digital Communications, 4th Edition*. McGraw-Hill, 2001.

[22] M. Rahriema and Y. Antia. Optimum soft decision decoding with channel state information in the presence of fading. *IEEE Communications Magazine*, 35(7):110–111, July 1997.

[23] A. Saleh and R. Valenzuela. A statistical model for indoor multipath propagation. *IEEE Journal on Selected Areas in Communications*, 5(2):128–137, Feb. 1987.

[24] H. Shafiee and S. Fouladifard. Calibration of iq imbalance in ofdm transceivers. In *IEEE International Conference on Communications*, volume 3, pages 2081–2085, May 2003.

[25] Standard. *Part 11: Wireless LAN Medium Access Control (MAC) and Physical Layer (PHY) specifications: High-speed Physical Layer in the 5 GHZ Band*. IEEE, 1999.

[26] A. Tanenbaum. *Computer Networks, Fourth Edition*. Prentice Hall, 2002.

[27] D. Tse and P. Viswanath. *Fundmentals of Wireless Communication*. Cambridge, 2005.

[28] A. W. van den Enden and N. Verhoeckx. *Digitale Signaalbewerking*. Delta Press BV, 1987.

[29] W. J. van Houtum. Personal communication. Technical report.

[30] W. J. van Houtum. On understanding the performance of the ieee 802.11a wlan physical layer for the gaussian channel. In *24-th Symposium on Information Theory in the Benelux*, MAY 2003.

[31] W. J. van Houtum. *PHD Wim*. PhD thesis, TU/e, 2006.

[32] R. van Nee and R. Prasad. *OFDM for Wireless Multimedia Communications*. Artech House, Inc., Norwood, MA, USA, 2000.

[33] J. Yoshida. Philips demos wireless network with wi-lan. http://www.eetimes.com/story/OEG19990827S0032.

Abbreviations

AC	alternating current
AD	analog digital
AGC	automatic gain control
AV	audio video
AWGN	additive white Gaussian noise
BER	bit error rate
BPSK	binary phase shift keying
CCK	complementary code keying
CHC	channel correction
CHest	channel estimation
COFDM	coded orthogonal frequency division multiplexing
cordic	COordinate Rotation DIgital Computer
CPE	common phase error
CRE	corporate research exhibition
CRC	cyclic redundancy check
CSI	channel state information
DA	digital analog
DAB	digital audio broadcasting
DBPSK	differential binary phase shift keying
DC	Direct Current
DFT	discrete Fourier transform
DSSS	direct sequence spread spectrum

DSP	digital signal processor
DQPSK	differential quadrature shift keying
DVB-T	digital video broadcasting terrestrial
ENOB	effective number of bits
EVM	error vector magnitude
FIR	finite impulse response
FCC	Federal Communications Commission
FEC	forward error correction
FFT	fast Fourier transform
FFC	feed forward correction
FPGA	field programmable gate array
FHSS	frequency hopping spread spectrum
I	in-phase
ICI	inter carrier interference
IDFT	inverse discrete Fourier transform
IEEE	Institute of Electrical and Electronics Engineers
IFFT	inverse fast Fourier transform
IF	intermediate frequency
IFA	Internationale Funkausstellung
IR	infra-red
ISI	inter symbol interference
ISO	International Organization for Standardization
ISM	industrial scientific and medical
LPF	low pass filter
LLR	log-likelihood ratio
MAC	medium access control
MIMO	multiple input multiple output
MISO	multiple input single output
MMSE	minimal mean square error

MPEG	Moving Picture Experts Group
MRC	maximum ratio combining
OFDM	orthogonal frequency division multiplexing
PER	packet error rate
PC	personal computer
PCB	printed circuit board
PHY	Physical layer
PRBS	pseudo random bit sequence
Q	quadrature
QAM	quadrature amplitude modulation
QOS	quality of service
QPSK	quadrature phase shift keying
RDI	receive data interface
RMS	root mean square
RF	radio frequency
RT-CV	real-time concept validator
SCI	serial control interface
SLE	System Laboratory Eindhoven
SIR	signal to interference ratio
SIMO	single input multiple output
SISO	single input single output
SNR	signal to noise ratio
SRC	sample rate converter
TCP/IP	transmission control protocol / internet protocol
VSA	vector signal analyzer
WLAN	wireless local area network
ZF	zero forcing

Appendix A

Error Vector Magnitude

The error vector magnitude (EVM) is defined in the standard [25, p. 30]. The formula is very specific, but can be generalized with equation A.1. In this equation S_k is the transmitted symbol and the $\hat{S_k}$ is the estimated received symbol.

$$EVM_{RMS} = \frac{E[\Re(S_k - \hat{S}_k)^2 + \Im(S_k - \hat{S}_k)^2]}{E[S_k S_k^*]} \tag{A.1}$$

Figure A.1 shows a block diagram, which is used for measuring the EVM. This means that there is a floating- point transmitter, which will generate a test vector. This will be processed by a fast Fourier transform (FFT) and a floating-point zero forcing (ZF) equalizer.

This means that the output signal of the FFT is:

$$R_k = H_k S_k + N_k \tag{A.2}$$

Signal R_k is the received signal for each sub-carrier and Nt_k the noise on that sub-carrier. In this equations the noise is a complex white Gaussian noise. In the following equations we assume that these variable N_k and $N_k^{(\times)}$ have got the same statistical properties, but are uncorrelated. This offset is a time offset which is applied to prevent the system against inter symbol interference (ISI). The FFT window will start in the cyclic prefix. In this model we have an AWGN channel model. This means that the estimated channel response is:

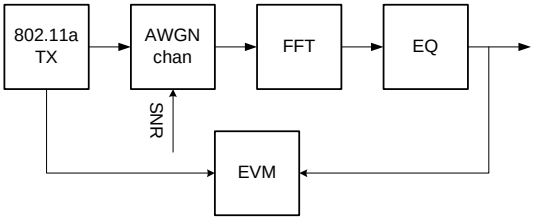

Figure A.1: block diagram of EVM measurements

$$\hat{H}_k = \frac{R_k}{L_k} = \frac{H_k L_k + N_k^{(1)}}{L_k} = H_k + \frac{N_k^{(1)}}{L_k} \tag{A.3}$$

This estimation is done based on the long training sequence (L_k). The training sequence consist of sub-carriers with a magnitude of 1. If we assume that we average the P training sequences. The estimation will be:

$$\hat{H}_k = H_k + \sqrt{1/P} \cdot \frac{N_k^{(2)}}{L_k} \tag{A.4}$$

The sent signal will be estimated with a zero-forcing equalizer. This means this estimation will be:

$$\hat{S}_k = \frac{R_k}{\hat{H}_k} \tag{A.5}$$

$$= \frac{H_k S_k + N_k^{(3)}}{H_k + \sqrt{1/P} \cdot \frac{N_k^{(2)}}{L_k}} \tag{A.6}$$

We can now calculate the EVM:

$$EVM_{RMS} = \frac{E\|S_k - \hat{S}_k\|^2}{E[\|S_k\|^2} \tag{A.7}$$

$$= \frac{E\left\| S_k - \frac{H_k S_k + N_k^{(3)}}{H_k + \sqrt{1/P} \cdot \frac{N_k^{(2)}}{L_k}} \right\|^2}{E\|S_k\|^2} \tag{A.8}$$

$$= \frac{E\left\| \frac{\sqrt{1/P} \cdot S_k \frac{N_k^{(2)}}{L_k} - N_k^{(3)}}{H_k + \sqrt{1/P} \cdot \frac{N_k^{(2)}}{L_k}} \right\|^2}{E[\|S_k\|^2} \tag{A.9}$$

$$= \frac{E\left\| \frac{\sqrt{1/P} \cdot S_k N_k^{(2)} - L_k N_k^{(3)}}{L_k H_k + \sqrt{1/P} \cdot N_k^{(2)}} \right\|^2}{E\|S_k\|^2} \tag{A.10}$$

If we assume a additive white Gaussian noise (AWGN) channel where H_k has a magnitude of 1. It is also clear that the magnitude of L_k is 1. Then we can assume that the factor $\sqrt{1/P} \cdot N_k^{(2)}$ is much smaller than the factor $L_k H_k$. With these assumptions we could approximate the EVM value:

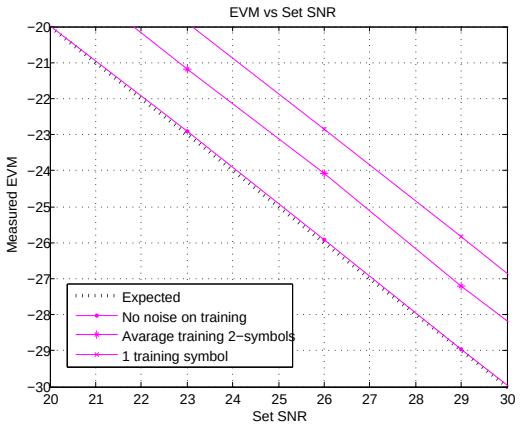

Figure A.2: EVM for different channel estimation methods

$$EVM_{RMS} \approx \frac{E\left\|\sqrt{1/P}\cdot N_k^{(2)} - N_k^{(3)}\right\|^2}{E\|S_k\|^2} \tag{A.11}$$

$$\approx (1+1/P)\frac{E\|N_k\|^2}{E\|S_k\|^2} = (1+1/P)\frac{1}{SNR} \tag{A.12}$$

If we do a simulation with a simple AWGN channel and a floating-point transmitter and we calculate the EVM. We would expect a relation between EVM and signal to noise ratio (SNR) which is in Equation A.12. The simulations are done based on a sufficient number of symbols, which is defined in the standard [25, p. 30].

The results of this simulation are plotted in Figure A.2, which contains four curves. The first curve is the expected curve ($P = \infty$). This curve assumes that the estimation of the channel response is perfect ($\hat{H}_k = H_k$). The second curve is based on a so-called super training symbol, were no noise is added to the long training sequence. The third curve is based on the real Tahoe implementation, which average the two OFDM-symbols of the long training sequences ($P = 2$). This will give an 1.7dB loss compared to the super training ($10\log_{10} 1.5$). If the channel estimation is based on a single orthogonal frequency division multiplexing (OFDM)-symbol ($P = 1$), there will be a 3dB loss and this is the last curve.

The lost in EVM is due to the effect that the received channel estimation still contains noise. If we use the term EVM in this thesis, this will always be based on the EVM curve with $P = 2$. The channel estimation is done based on the average of two OFDM training symbols. Equation A.13 shows the relation of SNR and EVM.

$$EVM(dB) = -SNR(dB) + 1.7dB \tag{A.13}$$

Appendix B

IQ-Imbalance

A complex base-band signal consists of two signals an in-phase (I) and quadrature (Q) signal (see B.1). In this section there will be a numerical analysis on two effects, which could occurs in measurements which are done in this thesis. In the digital domain the operations done on these two signals could be done exactly the same, without any deviance between the operation on the I or Q. If we do operations on these signals in the analog domain there will be deviation, because for example filters are never exactly the same. In Parot [18] and Shafiee [24] there are more detailed description of these effects and calibration methods.

$$s(t) = I(t) + \jmath Q(t) \tag{B.1}$$

B.1 Gain Mismatch

The first effect which could occur is gain mismatch, between the I and Q signal. This error can occur due to differences in gain of the analog digital (AD) converter, but it can also can come from differences from analog amplification or attenuations in the I or Q part of the analog base-band processing.

The gain mismatch can be written in a relative number ϵ. The I and Q value are multiplied with a gain depending on this relative number. Equation (B.2) is used as basis formula of gain mismatch for simulation and calculations.

$$\hat{s}(t) = (1+\epsilon)\, I(t) + \jmath\,(1-\epsilon)\, Q(t) \tag{B.2}$$

$$s_(t) \quad = \quad \begin{cases} \sum_{n=-N/2}^{N/2-1} a_n e^{\jmath\omega_n t} & \text{if } -\tau < t < \tau \\ 0 & \text{elsewhere} \end{cases} \tag{B.3}$$

An orthogonal frequency division multiplexing (OFDM) signal can be written as summation of complex orthogonal tones (see Equation B.3). were a signal $s(t)$ contains different sub-carriers ω_n. The data can be represented as complex number a_n. In the following calculations we will do calculations on one of the sub-carrier (see equation B.4).

$$s(t) = a_n e^{\jmath\omega_n t} = a_n \left(cos(\omega_n t) + \jmath sin(\omega_n t)\right) \tag{B.4}$$

When adding a gain mismatch to the signal, it will give the equation B.5.

$$\hat{s}(t) = a_n \left((1+\epsilon)cos(\omega_n t) + \jmath(1-\epsilon)sin(\omega_n t)\right) \tag{B.5}$$

This can be rewritten in complex terms of.

$$\hat{s}(t) = a_n \left(\frac{(1+\epsilon)}{2} \left(e.^{\jmath\omega_n t} + e^{-\jmath\omega_n t}\right) + \jmath \frac{(1-\epsilon)}{2\jmath} \left(e^{\jmath\omega_n t} - e^{-\jmath\omega_n t}\right) \right) \tag{B.6}$$

This gain mismatch will result into:

$$\hat{s}(t) = a_n \left(e^{\jmath\omega_n t} + \epsilon e^{-\imath\omega_n t}\right) \tag{B.7}$$

This means that this error will give an inter carrier interference (ICI). The information of the wanted carrier will leak into the the inverse frequency carrier. If we take $\epsilon = 1$ the complex base-band signal will be real, the complex term is zero. The signal $\hat{s}$ will be the addition of the positive and negative carrier. The signal to interference can be calculated, if we take the leakages as an interfering signal.

$$SIR_{GAIN} = \frac{1}{\epsilon^2} \tag{B.8}$$

The error vector magnitude (EVM) of the system can be calculated and will be $EVM = 10log_10(\epsilon^2) + 1.7dB$. In Figure B.1 shows the results of a simulation and calculation of the EVM for a different gain mismatches. The simulation is done with the simulation model, which is discussed in Appendix A on page 77. The calculation is done based on Equation B.8. It is clear that the results of these two methods are in the same order.

The calculated curve in Figure B.1 a 1.7dB channel estimation penalty is taken in account. In the simulations it is bit worse than expected.

The gain mismatch can be measured, this because equation B.9 is true for OFDM modulation, if there is no gain mismatch. If there is a gain mismatch, the different between both of the powers indicates the gain mismatch. This method is used to calibrate the measurement setup. The following expressions show how to estimate the gain error ϵ:

$$E(I^2(t)) = E(Q^2(t)) \tag{B.9}$$

$$\frac{E(\hat{I}^2(t))}{E(\hat{Q}^2(t))} - 1 = \frac{(1+\epsilon)^2 E(I^2(t))}{(1-\epsilon)^2 E(Q^2(t))} - 1 \tag{B.10}$$

$$= \frac{(1+\epsilon)^2}{(1-\epsilon)^2} - 1 \tag{B.11}$$

$$\approx \frac{1+2\epsilon}{1-2\epsilon} - 1 \qquad |\epsilon| \ll 1 \tag{B.12}$$

$$\approx \frac{4\epsilon}{1-2\epsilon} \approx 4\epsilon \tag{B.13}$$

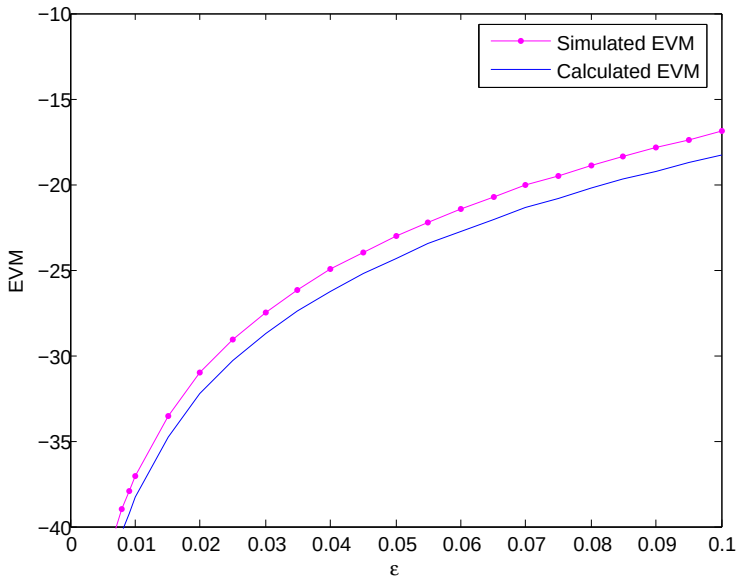

Figure B.1: Effect of gain error on OFDM system

As last remark is that the gain mismatch must be frequency independent. If this is not the case, this method of obtaining the gain mismatch is incorrect.

B.2 Phase Mismatch

The second IQ-imbalance is phase mismatches. If we look to the gain error it can be easily compensated by observing the powers of the I and the Q signals. If we take a phase mismatch then it means that signal from equation B.4 has got a phase error. In equation B.14 this error is applied.

$$\hat{s}(t) = a_n \left(cos(\omega_n t + \varphi) + \jmath sin(\omega_n t - \varphi) \right) \tag{B.14}$$

If we calculate what effect this error gives by calculating the back to the exponential terms:

$$\hat{s}(t) = a_n \left(\frac{1}{2} \left(e^{\jmath(\omega_n t + \varphi)} + e^{-\jmath(\omega_n t + \varphi)} \right) + \jmath \frac{1}{\jmath 2} \left(e^{\jmath(\omega_n t - \varphi)} - e^{-\jmath(\omega_n t - \varphi)} \right) \right) \tag{B.15}$$

This will give two components, the wanted and the leakage component:

$$\hat{s}(t) = a_n \left(\frac{e^{\jmath\varphi} + e^{-\jmath\varphi}}{2} \left(e^{\jmath\omega_n t} \right) - \frac{e^{\jmath\varphi} - e^{-\jmath\varphi}}{2} \left(e^{-\jmath\omega_n t} \right) \right) \tag{B.16}$$

This can be written in cosine and sine terms for the wanted and the interfering term.

$$\hat{s}(t) = a_n \left(\cos\varphi \left(e^{\jmath\omega_n t} \right) - \jmath \sin\varphi \left(e^{-\jmath\omega_n t} \right) \right) \tag{B.17}$$

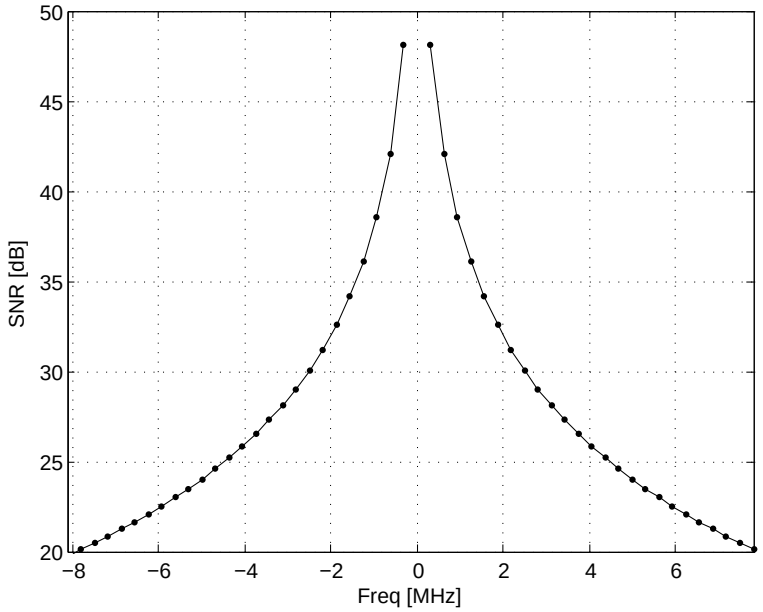

Figure B.2: SIR based on a 2ns delay

The signal to interference ratio (SIR) of the phase different can be written as:

$$SIR_{PHASE} = \frac{\cos^2(\varphi)}{\sin^2(\varphi)} \approx \frac{1}{\varphi^2} \tag{B.18}$$

For small value of φ the SIR can be linearly approximated. That is done in B.18. This means that the SIR quadratic with the phase difference of the IQ signals.

A phase shift can be written in terms of a delay. Equation B.19 shows this relation. In specification of the AD converter a maximum delay between the converters could be 2ns (datasheet [2]). Figure B.2shows the worst-case SIR with such a delay. This picture shows that the delay will have a frequency dependent SIR.

$$\varphi = \tau\omega_n \tag{B.19}$$

From Figure B.2 it is clear that, if the delay is 2ns the SIR of this chip is unacceptable low. As a conclusion of this observation, that this error has to be compensated.

Appendix C

Common Phase Error

In Chapter 5 on page 49 a new proposal of the equalizer is introduced. Only there is no discussion of the feed forward correction (FFC). In this Appendix there will be a discussion about the implemented FFC and a proposal of a new FFC. This will complement the new equalizer proposal.

The CPE correction is implemented in the FFC in the equalizer of the Tahoe. The FFC will take the information from the pilots and will be used for correcting the common phase error (CPE). Figure C.1 shows the block diagram of this algorithm. The left side contains the implementation of the Tahoe and right side an improved version of this detector and will be discussed later.

This correction loop will correct the remaining frequency error, which is not corrected, with the frequency error estimator in the synchronization unit. It will also correct the low frequency phase-noise see Piazzo [20], Abhayawardhana [3] and Petrovic [19].

Figure C.2 at the left side shows the effect of the remaining frequency error in terms of error vector magnitude (EVM). If we plot the constellation then it is clear that the constellation has got a CPE (see Figure C.3). Equation C.1 is a received signal, which got a CPE. If we apply a CPE correction to the signal and simulate the EVM, it only has got the remaining inter carrier interference (ICI). This effect is plotted in curve C.2 at the right side. Equation C.1 does not contain the effect of ICI. We assume that the frequency estimation in the synchronization is sufficient enough, so that this effect can be neglect.

$$R(n)_k = H_k S_k e^{\jmath\varphi n} + N_k \tag{C.1}$$

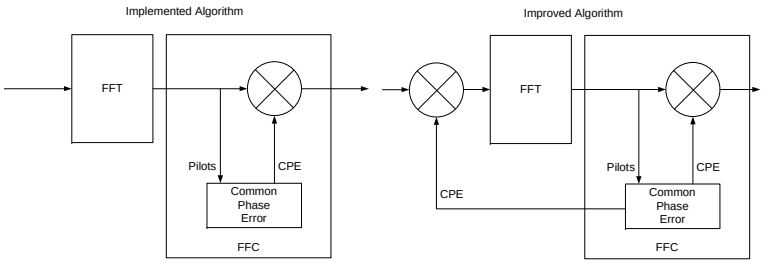

Figure C.1: Tahoe feed forward correction

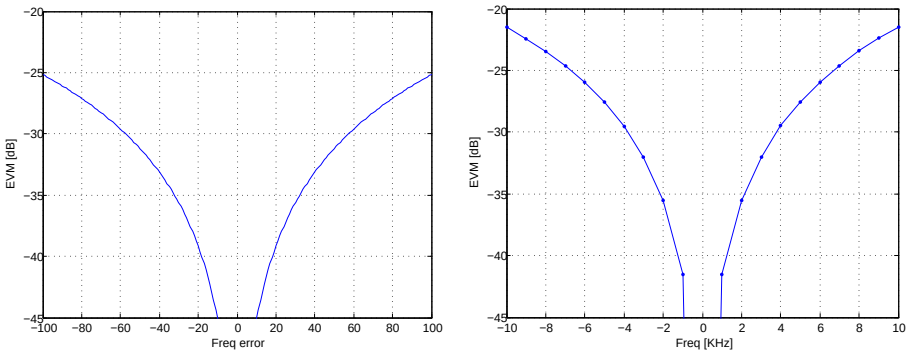

Figure C.2: The effect of CPE

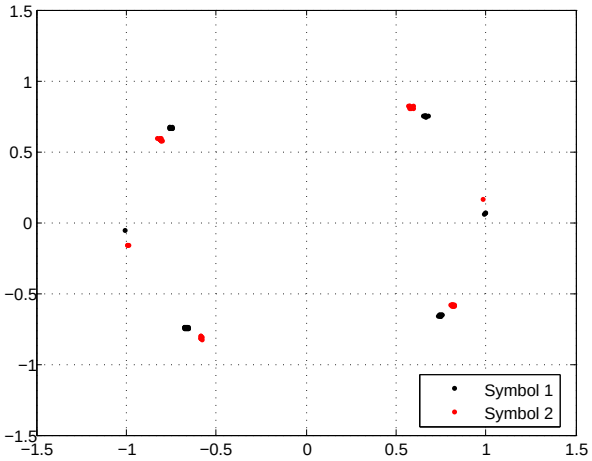

Figure C.3: QPSK constellation including pilots with frequency error

The feed-forward block in the Tahoe equalizer is correcting this CPE in frequency domain, this means that the remaining ICI is still in the signal. The implementation will average the phase of the equalized and decoded pilots (See equation C.2). The pilots which has got a magnitude under a certain threshold will not be used in this calculation.

$$CPE_n = E\left(\arg(\hat{S}_k) - \arg(S_k)\right) \tag{C.2}$$

A better estimation of the CPE is in equation . In this equation the received pilots are R_k. In IEEE 802.11a there are 4 pilots. S_k is the send pilots. $\hat{H}_k$ is the estimated channel response. This method is a maximum ratio combining (MRC) method of combining the pilots. The pilots who have more magnitude will have larger influence and pilots with smaller magnitude will have less influence on the final CPE.

$$\begin{aligned} \hat{CPE}_n &= \arg\left(\sum_{k=0}^{4-1} \frac{\hat{H}_k^* R_k}{S_k^*}\right) && \text{(C.3)} \\ &= \arg\left(\sum_{k=0}^{4-1} \frac{\hat{H}_k^* (H_k S_k e^{\jmath\varphi n} + N_k)}{S_k^*}\right) && \text{(C.4)} \\ &= \arg\left(\sum_{k=0}^{4-1} \hat{H}_k^* H_k e^{\jmath\varphi n} + \frac{\hat{H}_k^* N_k}{S_k^*}\right) && \text{(C.5)} \end{aligned}$$

If the absolute CPE value is large, this error have to be compensated in time domain. This compensation will reduce the ICI. The proposed algorithm will do a feed-forward correction in the frequency domain and a feedback correction in the time domain. This structure is shown in Figure C.1 at the right side.